Heme Acquisition in Campylobacter jejuni using the Chu Heme Transport System and its Role in Colonization and Pathogenesis.

A Thesis Presented for the

Master of Science

Degree

The University of Tennessee, Knoxville

Vincent Robert Randaisi

May 2025

Acknowledgements

I would like to express my deepest gratitude to my principal investigator, Dr. Jeremiah Johnson, for his continued support, guidance, and mentorship throughout this research journey. His knowledge and encouragement meant the world to me. I believe I would not be half the scientist I am today without his mentorship. I am deeply grateful to my professional committee members, Dr. Lindsey Burcham, Dr. Elizabeth Fozo, and Dr. Andrew Monteith, for their instructive feedback, constructive critique, and continuous support. Their expertise contributed significantly to the success of this thesis.

I am grateful to Dr. Andrew Monteith, who has provided superb guidance and sustained support in my research career. His acceptance as an additional graduate student enabled me to complete my research, for which I am truly thankful. Expertise, patience, and generosity have been invaluable to Dr. Monteith; his mentorship greatly enhanced my academic experience. Thanks for believing in me and providing me with all the resources I needed to finish my work. I would like to thank my collaborators, Dr. William Beavers, Brian Hachey, and Madison Bunch, for their encouragement and help with the sample analysis. Their contributions have proven to be invaluable in advancing my research.

I would also like to express my thanks to undergraduates Ryan Mesler and Nikki Vaccaro for their diligent work in preparing media and experiments. Their help was substantial in bringing this project to completion. I would also like to thank everyone in the UTK Microbiology department for their help in managing and encouraging students to go the extra mile to grow as scientists. Lastly, I would like to thank all my colleagues, friends, and family for their encouragement and support during the journey.

Abstract

This paper investigates the *Campylobacter jejuni* Chu heme transport system and its impact on pathogenesis. *Campylobacter jejuni* is one of the most common causes of bacterial gastroenteritis. The ability of *C. jejuni* to take up iron is an important factor in survival, particularly under low-iron conditions. For this purpose, the *chu* operon encoding *chuA, chuB, chuC*, and *chuD* was investigated by generating specific knockout mutants. Growth experiments tested these mutant strains' capabilities *in vitro* under iron-restricted conditions with heme supplementation. Furthermore, the C57BL6 IL-$10^{-/-}$ knockout mice were employed to assess the role of these genes *in vivo*. The ChuA heme receptor was identified as essential for growth under iron-limited conditions, while other genes in the operon demonstrated compensatory mechanisms. *In vivo*, all *chu* knockout strains exhibited significantly reduced fitness compared to wild-type *C. jejuni*, indicating that disrupted heme uptake adversely affects microbial survival. Furthermore, organ-specific differences in *chu* gene expression suggest that host factors, including diet, microbiome composition, and immune interactions, play critical roles in the fitness of *chu* knockout mutant strains.

Table of Contents

Chapter I - Introduction……1

Campylobacter jejuni……2

Intestinal Colonization……4

Innate Immune Activation……7

Neutrophils……9

Macrophages……11

Heme Uptake……13

Chapter II – Experimental Findings……14

Introduction……17

Material and Methods……21

Results……30

Chapter III- Discussion……43

Future Directions……50

References.……51

Appendix……64

Vita……71

List of Tables

Table 1: List of qPCR Primers……**69**

Table 2: Representation showing the qPCR analysis of the *chuA* gene across each category of sample……..…….**70**

List of Figures

Figure 1: *Campylobacter jejuni* Chu Mechanism 20

Figure 2: Mutant Growth Severely Impacted When Heme is the Sole Iron Source..... 31

Figure 3: Colonization of *C. jejuni* wild-type and *chu* mutant strains in different intestinal compartments of IL-10 deficient mice 33

Figure 4: Relative expression of *chuA* in wild-type *C. jejuni* across different intestinal compartments and feces 36

Figure 5: Human Heme Levels are elevated in *C. jejuni* infected stool..... 37

Figure 6: Biliverdin Levels Suggests Impaired Heme Metabolism 39

Figure 7: Histological analysis of intestinal pathology in the cecum and colon across experimental groups 41

Figure 8: Colonization Trends Over 10-Day Infection 64

Figure 9: Immune cell infiltration in IL-10 deficient mice infected with *C. jejuni* wild-type and *chu* mutant strains..... 65

Figure 10: Invasion Assay Shows No Significant Difference Between Wild-type *C. jejuni* and Δ*chu* Knockout Mutant Strains 66

Figure 11: Assay Shows No Significant Difference Between Wild-type *C. jejuni* and Δ*chu* knockout mutant strains..... 67

Figure 12: Motility Assay of Various Mutant Strains Over 24 and 48 Hours 68

Chapter I

Introduction

This chapter was written by V.R.R. and was based off a constructed skeletal outline edited by J.G.J and A.J.M.

Campylobacter jejuni

Campylobacter jejuni is a Gram-negative, microaerophilic bacterium that exhibits a distinctive spiral or curved rod morphology, measuring 0.2-0.8 μm in width and 0.5-5 μm in length (1). *C. jejuni* represents a significant global health concern, with surveillance data indicating approximately 400-500 million infections annually worldwide (2). In the United States alone, *C. jejuni* accounts for 88.4% of all *Campylobacter* infections, making it the predominant species responsible for human campylobacteriosis, with many more undocumented cases expected to go undiagnosed each year (3,4). The economic impact is substantial, with annual costs estimated at $1.7 billion in the United States alone (5). The next most common disease-causing *Campylobacter* is *Campylobacter coli,* at approximately 10-20% of *Campylobacter* disease cases (6,7). Given the extremely high percentage of human cases involving *C. jejuni*, it remains the most significant clinical concern.

Transmission of *C. jejuni* primarily occurs through the ingestion of contaminated food, primarily poultry, contaminated water, and unpasteurized milk (3,8). The microaerophilic nature of *C. jejuni* reflects its evolutionary adaptation to specific host environments. *C. jejuni* requires oxygen concentrations between 5-10% and colonizes the gastrointestinal tract of avians, mammals such as cattle and other livestock, as well as humans. In the small intestine, *C. jejuni* colonizes the duodenum and jejunum. In the large intestine, *C. jejuni* colonizes that colon. *C. jejuni* demonstrates optimal growth at temperatures ranging from 37°C to 42°C (8–11). This temperature range corresponds precisely to the physiological temperatures of its primary hosts, humans whose physiological temperature is 37°C and poultry, which possess elevated core

temperatures at 42°C. *C. jejuni* is considered a commensal in avian species and commonly resides within the gastrointestinal tract without causing disease (3,8). Temperature is a driving factor for a lack of pathogenesis, certain virulence factors, such as outer membrane vesicles (OMVs) are downregulated at 42°C and upregulated at 37°C (12). One of the most prominent OMV is cytolethal distending genotoxin (CDT), which causes DNA double-strand breaks and cell cycle arrest (13), which in turn, increases the risk of developing cancer. Additionally, the infectious dose for *C. jejuni* is low, with as few as 500 bacterial cells capable of establishing infection in humans (12). This low infectious dose, combined with the organism's widespread presence in the food supply, contributes to its high incidence rate even in developed countries.

The clinical presentation of *C. jejuni* infection varies significantly among individuals. Acute gastroenteritis typically manifests with severe abdominal pain, bloody diarrhea, and fever, persisting for 5-7 days (14–16). In most cases, immunocompetent individuals will clear the infection on their own without the need of antibiotic intervention. Young children, the elderly, and immuno-compromised individuals are more at risk for developing post-infectious complications from *C. jejuni* infections (17). This is likely due to having a reduced immune cell count to efficiently fight *C. jejuni.* One complication is post-infectious irritable bowel disease (PI-IBD) (18). PI-IBD can cause persistent diarrhea, abdominal pain, weight loss, fatigue, and rectal bleeding. The persistent inflammation caused by PI-IBD can lead to long-term damage to the gastrointestinal tract and can lead to continuous cellular turnover, increased reactive oxygen species (ROS) presence, and DNA damage, which all can contribute to the development of cancer over time by a host derived immune response (18,19). If tumorigenesis occurs as a result, it can be beneficial for *C. jejuni*. Tumors undergo an increased rate of glycolysis, in a process known as the Warburg effect (20), where cancer cells preferentially utilize glycolysis even in the

presence of oxygen. As a result, high levels of lactate accumulate in the tumor microenvironment, reaching concentrations of 10-30 mM, which allows *C. jejuni* to utilize lactate as a carbon source through its lactate dehydrogenase (LDH) and lactate permease systems (21).

C. jejuni infections can also result in severe autoimmune complications. Guillain-Barré syndrome (GBS), characterized by progressive muscle weakness and paralysis (22). *C. jejuni's* cell wall contains lipooligosaccharides (LOS), which mimic host glycosylation patterns, aiding in immune evasion and increasing the host's risk for developing GBS (22,23) In patients suffering from GBS, up to 40% of GBS cases can be linked to *C. jejuni* (22). Post-infectious reactive arthritis (RA) is another significant complication, affecting 1-5% of *C. jejuni* infected individuals (24). The sequela results from *C. jejuni* are likely the result of the host immune response to *C. jejuni*, rather than the bacteria itself. The exaggerated immune response begins during the colonization of the human host's gastrointestinal tract.

Intestinal Colonization

Once ingested, *C. jejuni* migrates to the host's gastrointestinal tract. Once there, *C. jejuni* migrates towards the mucus layer of the small and large intestine to colonize. Colonization relies heavily on *C. jejuni*'s distinctive motility mechanisms. *C. jejuni's* helical shape, combined with amphitrichous flagella, enables efficient penetration of intestinal mucus layers through corkscrew-like motility (11). *C. jejuni* can actively modify its swimming behavior in response to the varying viscosity of intestinal mucus (25). In contrast to numerous other pathogenic gastrointestinal pathogens, such as *Salmonella* spp., (15). For example, *C. jejuni* lacks a traditional type III secretion system (T3SS) and instead utilizes specialized flagella for protein secretion, referred to in the literature as flagellar-associated T3SS. (9,26). In *C. jejuni,* flagella

serve multiple functions beyond motility and secretion, *C. jejuni's* flagella also acts as a T3SS's for the delivery of virulence factors into host cells (27,28). Additionally, the flagella also play a role in biofilm formation, adherence, cellular invasion of intestinal epithelial cells (IEC's) (9,29).

Following mucus penetration, *C. jejuni* employs a complex array of adhesion mechanisms to establish contact with host epithelial cells. Two key adhesins, CadF (*Campylobacter* adhesion to fibronectin) and FlpA (fibronectin-like protein A), specifically target host cell fibronectin, enabling firm attachment to the basolateral surface of intestinal epithelial cells (28,29). The expression of these adhesins is tightly regulated by environmental signals, including temperature and oxygen concentration, ensuring optimal attachment under host conditions (30)

The invasion process is facilitated by *C. jejuni*'s sophisticated protein secretion systems, particularly the flagellar-associated type III secretion system (T3SS). This system delivers effector proteins, including the *Campylobacte*r invasion antigens (Cia), directly into host cells, triggering actin, cytoskeletal rearrangements that promote *C. jejuni* internalization (31). *C. jejuni* is also capable of invading the lateral side of cells through tight junctions by secreting the serine protease HtrA, that cleave occluding and claudin-8 found within tight junctions (14,32,33). However, tumor necrosis factor-α (TNF-α) must be present for successful lateral cell invasion (34). When macrophages are recruited to the site of infection, macrophages secrete TNF-α to create a more inflammatory environment (35). As a result, *C. jejuni* can invade IEC at an increased rate. Upon *C. jejuni* invasion, IEC's secrete interleukin-8 (IL-8), resulting in neutrophil recruitment to the site of invasion, further increasing inflammation (32).

Critical to successful colonization is *C. jejuni*'s ability to acquire essential metals, particularly iron, from the host environment. *C. jejuni* has evolved sophisticated metal

acquisition systems, including the ChuABCD system for heme uptake and the Cj1658-Cj1663 genes encoding a ferric enterobactin uptake system (8,36). These systems are essential for overcoming nutritional immunity, which is the host's attempt to restrict metal availability to pathogens. These systems are orchestrated by two key regulators in *C. jejuni*: Fur (Ferric Uptake Regulator) and HeuR (Heme Utilization Regulator). Fur acts as a global regulator of iron homeostasis, while HeuR specifically controls the ChuABCD system by serving as a transcript factor, optimizing heme uptake during low iron conditions (37,38). Heme is an iron containing molecule and is a component of hemoglobin and myoglobin and serves many functions within the host. The center of the heme molecule contains a single iron atom. *C. jejuni* can utilize heme as an alternative iron source in iron-limited environments. *C. jejuni* possesses multiple potential mechanisms for iron acquisition. These include at least five predicted iron-binding proteins, two outer membrane receptors for ferric siderophores, two ABC transporter systems for iron uptake (comprising permeases and ATP transporters), a complete hemin uptake system (Chu), a ferrous iron transporter, and three TonB/ExbB/ExbD complexes (39). Having numerous iron acquisition systems demonstrates the metabolic importance that iron holds for *C. jejuni*. Iron has been found to play important roles in enzymatic functionality, cellular respiration, catalase production, and gene expression with 647 genes being found to be transcriptionally controlled by iron levels (8,40,41). Beyond its nutritional importance, iron availability also serves as a critical signal for pathogens to detect host invasion.

Iron metabolism in *C. jejuni* represents a delicate balance, as free iron can generate harmful reactive oxygen species (ROS) through Fenton chemistry (42). This necessitates tight regulation by both the host and pathogen. Iron availability significantly influences *C. jejuni*'s virulence profile, affecting protein glycosylation, motility, adhesion, and toxin production (40).

The glycosylation of surface proteins, critical for immune evasion and host interaction, requires iron as a cofactor (40). Additionally, iron-restricted conditions significantly impair *C. jejuni*'s colonization efficiency (43). Iron acquisition systems support the specialized motility and adhesion mechanisms that enable *C. jejuni* to penetrate the intestinal mucus layer and adhere to epithelial cells (39,48). Iron availability also regulates the expression of *Campylobacter* invasion antigens (Cia), which are delivered into host cells via the flagellar-associated type III secretion system (T3SS), facilitating bacterial internalization and pathogenesis (33).

Innate Immune Activation

Upon bacterial invasion of the intestinal epithelium, the innate immune system serves as the first line of defense, initiating a cascade of protective responses. This rapid immune activation is crucial for controlling bacterial spread and orchestrating the subsequent adaptive immune response. This recognition process marks the beginning of a complex host-pathogen interaction that shapes the course of infection.

A pivotal aspect of the initial immune response is the production of IL-8. *C. jejuni* infection induces significant IL-8 production through multiple pathways, including NF-κB activation and MAPK signaling (44). This IL-8 response serves as a primary signal for neutrophil recruitment, with studies showing that IL-8 levels directly correlate disease severity in human infections (45). The recruitment and activation of neutrophils represents a critical component of the host response to *C. jejuni*. *C. jejuni* stimulates neutrophil extracellular traps (NETs) formation through a novel mechanism involving the bacterial protein SliP, which modifies host histone H3 through deacetylation (15,46). This process not only affects chromatin structure but also influences transcriptional responses (15,46). Inexplicably, inflammation appears to be a prerequisite for successful *C. jejuni* colonization, as evidenced by studies using

IL-10 deficient mice. These mice, lack the anti-inflammatory cytokine IL-10, show enhanced susceptibility to *C. jejuni* infection compared to wild-type counterparts (47). The heightened inflammatory state in IL-10 deficient mice creates an environment that favors *C. jejuni* colonization, suggesting that *C. jejuni* has evolved to exploit inflammatory conditions.

The pathology of *C. jejuni* infections is driven by a combination of host immune responses and bacterial strategies that exploit inflammation. Innate immune cells, such as neutrophils and macrophages, play a central role in this process. Neutrophils generate reactive oxygen species (ROS) through NADPH oxidase activation, which are effective in killing pathogens but also cause collateral damage to host tissues (46,48). Additionally, neutrophils release nucleases, proteases, and elastases that degrade bacterial components and extracellular matrix proteins, further contributing to tissue damage and inflammation (15,46,48).

Goblet cells, which are specialized epithelial cells responsible for producing and secreting mucins, specifically, MUC2 in the intestinal tract (49). Mucins are critical for maintaining the intestinal mucus barrier. This barrier prevents bacterial adhesion to the epithelium and supports gut homeostasis. In addition, mucus production is reliant on interactions with microbes. In germ-free and antibiotic treated mice, gut mucus defects are a prevalent (50). During *C. jejuni* infection, significant goblet cell loss occurs however, there are no characterized virulence factors that *C. jejuni* possess to specifically target goblet cells. Goblet cell loss may be an indirect result of the host's immune response. When inflammation increases, goblet cells secrete mucus in response to aid in the protection of nearby cells in the gastrointestinal tract (51). Excessive or chronic inflammation can lead to goblet cell dysfunction, including decreased mucus production, altered mucus quality, and even cell death, which can exacerbate inflammation (51). The loss of goblet cells compromises the protective mucus layer, increasing

bacterial adherence to epithelial cells and enhancing susceptibility to secondary infections (51). This phenomenon is not unique to *C. jejuni* and has been observed in other gastrointestinal infections, where inflammation and tissue damage disrupt the epithelial barrier (52).

The inflammatory response to *C. jejuni* infection is characterized by edema and hyperplasia of the intestinal tissue. Edema results from increased vascular permeability and fluid accumulation, while hyperplasia reflects heightened epithelial cell proliferation in response to tissue damage (53). These pathological changes aids *C. jejuni*'s colonization, as inflammatory environments release heme from damaged erythrocytes at the site of inflammation during tissue damage (54). The bleeding that occurs provides a source of heme for bacterial iron acquisition; a mechanism observed in other enteric pathogens such as *Clostridioides difficile* (54)

Neutrophils

Neutrophils, a cornerstone of the innate immune system, are the most abundant type of white blood cells in human circulation, constituting approximately 50-70% of all leukocytes (62,63). In mice, neutrophils make up approximately 10-25% of the circulating leukocytes (57,58). Neutrophils are generated through a tightly regulated process known as granulopoiesis within the bone marrow. During this process, hematopoietic stem cells differentiate into myeloid progenitors, which subsequently mature into neutrophils under the influence of growth factors such as granulocyte colony-stimulating factor (G-CSF) (59). This process ensures a continuous supply of neutrophils, with the bone marrow producing an estimated 10^{11} neutrophils daily to meet the body's immunological demands (60). The critical role of G-CSF in neutrophil production is underscored by studies in mice lacking G-CSF or its receptor. These mice exhibit severe neutropenia, with drastically reduced neutrophil counts (61,62).

In peripheral blood, the average neutrophil count ranges from 2,500 to 7,000 cells per microliter. These numbers can fluctuate in response to infections, inflammation, or other physiological stressors (60). Neutrophils employ three primary mechanisms to combat pathogens: phagocytosis, where microbes are engulfed and destroyed within phagosomes; degranulation, which releases antimicrobial proteins such as defensins and myeloperoxidase; and the formation of neutrophil extracellular traps (NETs), composed of chromatin and antimicrobial molecules, which trap and neutralize pathogens (61). Additionally, neutrophils interact with other immune cells, such as macrophages and dendritic cells, by releasing cytokines like IL-8 and TNF-α, amplifying the inflammatory response and coordinating the innate and adaptive immune systems.

At infection sites, neutrophils deploy an arsenal of antimicrobial strategies against *C. jejuni*. The primary defense mechanisms include the secretion of potent antimicrobial enzymes, particularly myeloperoxidase (MPO) and neutrophil elastase, which target bacterial structural components (15,62). MPO catalyzes the production of hypochlorous acid and other reactive oxygen species, while also participating in NET formation to entrap and eliminate pathogens (64). However, *C. jejuni* possesses a DNA glycohydrolase, known as MugA, that dismantles NETs, enabling *C. jejuni* to escape from these extracellular traps (46).

Neutrophil elastase not only degrades bacterial adhesins and invasins but also exhibits strong DNA-binding properties, allowing it to associate with NETs and efficiently clear trapped pathogens (15). Beyond direct antimicrobial activities, neutrophils participate in nutritional immunity by deploying metal-binding proteins. The calgranulin S100A12 sequesters calcium, cooper, and most importantly zinc, which is a crucial cofactor for numerous *C. jejuni* metabolic processes, thereby inhibiting *C. jejuni* proliferation (63). Similarly, neutrophil-derived lipocalin-

2 interferes with bacterial iron acquisition by binding to enterobactin, forcing *C. jejuni* to rely more heavily on alternative iron sources, particularly host-derived heme compounds (15).

Macrophages

Macrophages are versatile and highly specialized cells of the innate immune system, playing a central role in host defense, tissue homeostasis, and immune regulation. Macrophages primarily originate from hematopoietic stem cells in the bone marrow, which differentiate into monocytes that circulate in the bloodstream. Upon migration into tissues, monocytes differentiate into macrophages, adapting to the local microenvironment to perform tissue-specific functions (65,66). In the gastrointestinal tract, a significant population of tissue-resident macrophages develops from embryonic precursors during fetal development and maintains itself through local proliferation, similar to other tissue-resident populations such as microglia in the brain and Kupffer cells in the liver (66,67).

Functionally, macrophages are key players in both innate and adaptive immunity, with distinct specializations in the gut environment. Within the intestinal mucosa, macrophages maintain a uniquely tolerant phenotype despite constant exposure to microbial stimuli and food antigens. These intestinal macrophages, particularly abundant in the lamina propria, express high levels of CX3CR1 and are characterized by their hypo responsiveness to bacterial products while retaining their phagocytic and bactericidal activities (68,69). This selective anergy prevents excessive inflammation in response to commensal microorganisms while maintaining protective immunity against pathogens. Beyond their traditional roles as professional phagocytes and antigen-presenting cells, gut macrophages actively participate in maintaining the integrity of the epithelial barrier and promoting tissue repair through the production of factors such as IL-10 and prostaglandin E2.

The significance of macrophages in intestinal homeostasis is particularly evident in their role in maintaining gut health and disease. In inflammatory bowel diseases (IBD), the balance of tolerogenic and inflammatory macrophage populations becomes disrupted, leading to inappropriate inflammatory responses (70). Their ability to polarize into distinct phenotypes, such as the pro-inflammatory M1 and anti-inflammatory M2 states, underscores their functional plasticity in response to environmental cues. The significance of macrophages extends beyond their role in infection and inflammation. They are implicated in the pathogenesis of various diseases, including cancer, atherosclerosis, and autoimmune disorders, where their dysregulated activity can exacerbate disease progression.

Additionally, macrophages play a central role in iron homeostasis, with hepcidin and ferroportin serving as key regulators. Hepcidin, a peptide hormone, controls iron levels by binding to ferroportin, the primary iron exporter in macrophages, enterocytes, and hepatocytes, leading to its degradation. This mechanism is crucial for systemic iron balance, as hepcidin levels adjust in response to iron stores and inflammatory signals (71). During *C. jejuni* infection, macrophages contribute to nutritional immunity by sequestering iron, thereby depriving the pathogen of this essential nutrient. This defense strategy involves upregulating iron-binding proteins like ferritin and downregulating ferroportin to limit iron availability when extracellular hemoglobin levels are elevated (72,73). All these factors influence *C. jejuni* colonization and with iron restriction, macrophages play a role in nutritional immunity.

Heme Uptake

Heme is an iron-containing porphyrin molecule that plays a critical role in various biological processes. It serves as a prosthetic group for numerous proteins, including hemoglobin, myoglobin, and cytochromes, facilitating oxygen transport, electron transfer, and enzymatic catalysis. The central iron atom in the heme allows it to participate in redox reactions, making it indispensable for cellular respiration and energy production. In addition to its role in host physiology, heme is a vital nutrient for many pathogens, as it provides a readily accessible source of iron, which is often limited during infection due to host-imposed nutritional immunity.

In *C. jejuni*, heme uptake is facilitated by the *Campylobacter* Heme Uptake (Chu) system and is encoded on the *chu* gene operon (*chuZABCD*) (8). The Chu system is comprised of several essential components that work in concert to facilitate heme uptake and utilization. ChuA, a TonB-dependent outer membrane receptor, specifically recognizes and binds heme molecules in the extracellular environment. The function of TonB receptors relies on their interaction with the TonB-ExbB-ExbD complex, which spans the bacterial inner membrane and periplasm and generate a proton motive force mediated by the ExbB and ExbD proteins (74). This complex provides the energy required for active transport across the outer membrane and into the periplasmic space. Once heme enters the periplasmic space, an unidentified hypothetical heme transport protein transports heme to the inner membrane ABC-transport system, which is comprised of the remaining Chu proteins.

ChuB is an inner membrane permease. Permeases contain multiple transmembrane α-helices that span the lipid bilayer, creating a specific channel or pore that facilitates heme movement across the inner membrane and into the cytoplasm (8,65). ChuC, the ATP-binding protein, generates energy via ATP hydrolysis to provide the necessary energy for the ChuB

permease to undergo the necessary confirmational change to allow heme into the cell (8,76). ChuD functions as a periplasmic heme-binding protein, which binds to heme once it is transported to the inner membrane by the unidentified transport protein (8). ChuBCD works together to incorporate heme through the inner membrane into the cytoplasm. Once internalized, ChuZ, a heme oxygenase, breaks down heme into biliverdin, carbon monoxide, and free iron, making the iron available for cellular processes (8). The *chuZ* gene is unique on the *chu* operon as it transversely transcribed.

In a study by Crofts and colleagues (2018), it was demonstrated that *chuA*, *chuD*, and *chuZ* are were the most significantly upregulated, 500-fold, iron sequestering genes during human infection compared to chicken colonization (77). As discussed in prior sections, *C. jejuni* does not cause disease in avian species. This differential expression highlights the importance of heme acquisition for *C. jejuni*'s in colonizing human hosts, potentially leading to pathogenesis in humans. The ability to acquire and utilize heme is shared among various gram-negative gastrointestinal pathogens. For instance, *Pseudomonas aeruginosa* employs the (*Pseudomonas* Heme Uptake) Phu system for heme uptake to acquire heme from their environment (78). The Phu (*Pseudomonas* heme uptake) system, first characterized in *Pseudomonas aeruginosa*, shares structural and functional similarities with the Chu system in *C. jejuni*, offering valuable insights into bacterial heme acquisition mechanisms.

Conclusions

Heme plays a pivotal role in the successful colonization of *Campylobacter jejuni* within the host. As the primary reservoir of iron in the host, heme is a critical nutrient that supports bacterial growth, metabolism, and the expression of virulence factors. The ability of *C. jejuni* to acquire heme through specialized systems, such as the Chu system, underscores its adaptation to

the iron-limited environment imposed by the host's nutritional immunity. Inflammatory responses, while aimed at controlling infection, inadvertently facilitate heme availability by inducing tissue damage and bleeding. This process not only provides a source of heme but also disrupts the intestinal barrier, further enhancing *C. jejuni's* colonization potential.

Destruction of goblet cells, which are essential for maintaining the mucosal barrier through mucus production, represents another consequence of inflammation that benefits *C. jejuni* colonization. The loss of these cells compromises the host's defense mechanisms, creating an environment conducive to bacterial persistence, be it direct targeting of goblet cells by *C. jejuni* or an unintended effect by macrophage regulation, remains to be investigated. Additionally, the interplay between iron acquisition and inflammatory responses highlights *C. jejuni's* reliance on host-derived nutrients for survival. Regulatory systems, such as Fur and HeuR, enable *C. jejuni* to optimize iron uptake and utilization, ensuring its metabolic needs are met even under restrictive conditions.

The interaction between *C. jejuni* and the host immune system further illustrates the complexity of its pathogenesis. Neutrophils and macrophages, key players in the innate immune response, attempt to limit bacterial proliferation through mechanisms such as nutritional immunity and the formation of neutrophil extracellular traps (NETs). However, the inflammatory environment, characterized by tissue edema and hyperplasia, paradoxically supports bacterial colonization by increasing nutrient availability and disrupting epithelial integrity in efforts to acquire heme-iron in iron-limited environments. These findings underscore the dual role of inflammation in both restricting and facilitating *C. jejuni* infection.

Chapter II

Heme Paper

This chapter is a version of a manuscript that is not yet published by Vincent Randaisi and Jeremiah G. Johnson titled “Heme Acquisition in *Campylobacter jejuni* using the Chu Transport System and its Role on Pathogenesis. Randaisi, V.R., Beavers, W.N., Johnson, J.G. (2024) *Heme Acquisition in Campylobacter jejuni using the Chu Transport System and its Role on Pathogenesis.* [unpublished manuscript] The work for this study was performed by the following individuals: Mutant generation, Mouse Colonization, qPCR, heme growth assays, motility assay, gentamycin protection assay, HCT116 cell culture, and histology analysis was performed by Vincent Randaisi, Theresa Rodgers, Tiara Ashurst, and Madison Bunch.

Introduction

Infection by *Campylobacter* species is a significant global health issue, causing an estimated 400 million cases of gastroenteritis each year, and resulting in substantial morbidity, mortality, and economic burden. Epidemiological studies have found that most individuals are infected with the species *C. jejuni*, and that they experience self-limiting moderate-to-severe gastroenteritis which is accompanied by inflammatory diarrhea and stomach pain. In addition to acute gastrointestinal diseases, campylobacteriosis is associated with long-term complications, including post-infectious irritable bowel syndrome, Guillain-Barré Syndrome, Miller-Fisher syndrome, and reactive arthritis. Despite the impact of these infections on human health, little is known about how the host responds to *Campylobacter* spp. and how the bacterium counteracts or promotes host responses to facilitate colonization, disease, and/or dissemination.

Nutritional immunity is a defensive mechanism used by hosts to restrict the access of vital nutrients to invading pathogens, including iron. For example, iron in host tissues is often found in complexes with host molecules, including heme, lactoferrin, and transferrin, leading free iron to be present from 10^{-24} to 10^{-7} M (79). During infection, this sequestration is further

contributed to by the immune-mediated release of iron-uptake promoting molecules like hepcidin and leukocyte-derived proteins like lipocalin-2 (Lcn2) (80). Several of these nutritional immunity factors are also present in the gastrointestinal tract, which is further impacted by iron complexing to dietary components and microbiota-derived molecules like siderophores. These processes effectively limit the growth and survival of pathogens in hosts and facilitate eventual clearance. For example, during campylobacteriosis, the Johnson lab and others have demonstrated that nutritional immunity factors like calprotectin, Lcn-2, and S100A12 are significantly increased in gastrointestinal lumen during infection (15,46).

Pathogenic bacteria have evolved several mechanisms to counteract nutritional immunity, including the acquisition of iron directly from several host molecules, including heme, lactoferrin, and transferrin (81,82). In heme utilization, a significant amount of research has focused on elucidating these mechanisms in Gram-positive pathogens, including *Staphylococcus aureus*, or in Gram-negative pathogens, like *Pseudomonas aeruginosa*. For example, the Phu system in *P. aeruginosa* is used to acquire nutritional iron from heme and is comprised of, PhuA, an outer membrane receptor that binds hemoproteins like hemoglobin and myoglobin; the TonB-dependent energy transducer, PhuR, which interacts with PhuA to transfer heme across the outer membrane; PhuT, which is a periplasmic heme chaperone; and the ABC transporter PhuVW, which translocate heme across the inner membrane into the cytoplasm (78). Similarly, *C. jejuni* encodes a heme utilization operon (*chuZABCD*) that was shown to facilitate growth in iron-restricted cultures when exogenous heme is added as an iron source. This study further found that heme-dependent growth relies on the heme oxygenase, *chuZ*, and the heme receptor, *chuA*, but not the inner membrane ABC transporter, *chuBCD*. In subsequent studies, *chuZABCD* were found to be upregulated in the feces of healthy volunteers infected during a human feeding study

(83). Since *chuZABCD* have been shown to be negatively regulated by the ferric-uptake regulator (Fur), this result suggests that the lower gastrointestinal tract possesses low-levels of free iron and that the acquisition of heme-derived iron may be required for colonization and/or growth.

While these molecular mechanisms of heme acquisition have been well-characterized in several pathogens, the specific role of these systems during host infection remained largely unclear. The knowledge gap was particularly intriguing for *C. jejuni*, given its unique niche as a foodborne pathogen that must adapt to both environmental and host conditions. The presence of a complete heme utilization system in *C. jejuni* raised compelling questions about its function during infection specifically, whether this system was merely advantageous or essential for establishing successful colonization in the gut. These questions became even more relevant considering the complex environment of the gastrointestinal tract, where multiple bacterial species compete for limited iron resources while facing host immune defenses.

To investigate whether heme utilization is required for gastrointestinal infection by *C. jejuni*, in-frame deletion mutant strains were constructed of the individual components of the transport system (ChuABCD) and examined their ability to acquire nutrient iron from heme under iron-restricted conditions (**Figure 1**). It was found that only the heme receptor, ChuA, was required for heme utilization and that the presumed cognate ABC transporter, ChuBCD, was not required for this process. Further investigation into the role of this system *in vivo*, determined that all determinants were required for efficient colonization and that, despite exhibiting reduced fecal and tissue burden, the mutant strains caused significant intestinal bleeding and pathology.

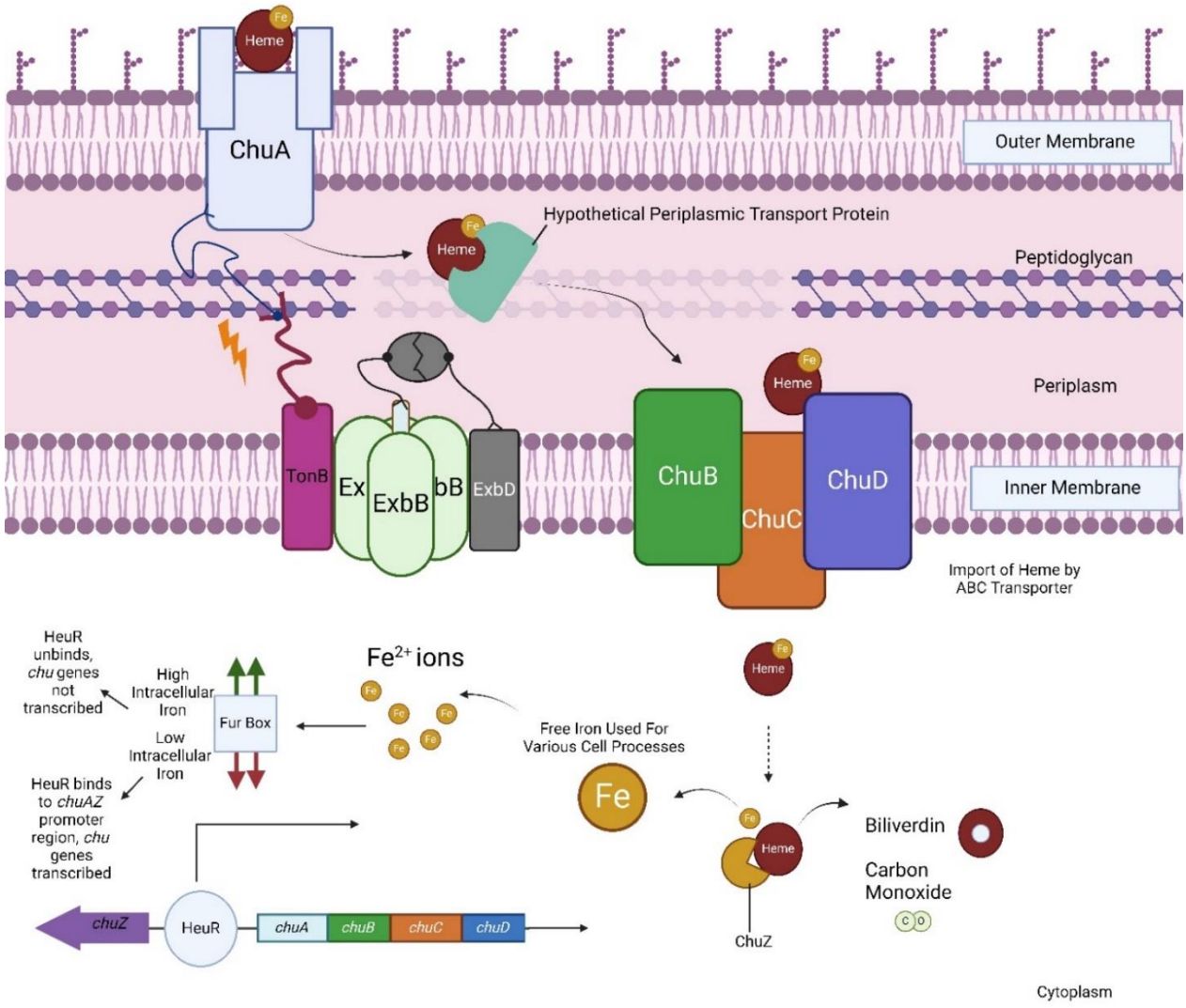

Figure 1: *Campylobacter jejuni* Chu Mechanism: Schematic for the overall proposed Chu system that *C. jejuni* utilizes. ChuA is a TonB-dependent outer membrane heme receptor. Heme is then transported into the periplasmic space via proton motive force and binds to an unidentified periplasmic transport protein. Heme is then delivered to the inner membrane ChuBCD complex. ChuB is an inner membrane permease, ChuC is an ABC transporter, and ChuD is a periplasmic hemin-binding protein. Figure created using Biorender.

Materials and Methods

Mutant Generation. Knockout mutants of *Campylobacter jejuni* 81-176 were generated using a systematic approach. Primers for the target gene were designed with IDT software, and overlapping primers were employed to amplify the gene region of interest via splicing by overlap extension PCR (SOE-PCR). SOE-PCR approach was specifically chosen for its ability to create precise gene deletions without introducing unwanted mutations at the junction sites. A touchdown PCR protocol with annealing temperatures (starting at 65°C and decreasing by 0.5°C per cycle for 20 cycles) was utilized to maximize specificity and yield during fragment stitching. The resulting stitched PCR products were ligated into the pJET1.2 plasmid vector using CloneJET PCR Cloning Kit (ThermoFisher Scientific, Cat. # K1231) following the manufacturer's instructions.

The ligated product was transformed into competent Max Efficiency DH5α cells (ThermoFisher Scientific, Cat. # 18258012) via electroporation. 15 µL of plasmid DNA to each tube was added. For the negative controls, 15 µL of nuclease-free water was added. Tubes were placed in ice for 30 minutes. Cells were then added to chilled electroporation cuvette and shocked at 2.5 kV (EC2 setting). 55 µL of MH broth was immediately added to the cuvette and cells were placed on ice for 10 minutes. Potential transformants were transferred to 1.5 mL Eppendorf tubes. Following the transfer, 500 µL of Super Optimal broth with Catabolite repression (S.O.C.) Medium (ThermoFisher Scientific, Cat. # 15544034) was added. Cells were immediately incubated at 37ºC and shaken at 200 rpm for 1 hour. Transformants were plated onto Lysogeny Broth (LB) with Ampicillin media plates and grown up at 37ºC overnight. Colonies were picked and screened using colony PCR to confirm the presence of the insert, and positive colonies were subjected to plasmid purification for sequencing to verify the accuracy of

the insert. Afterwards, both the pJET-stitched product and the plasmid pGEM-*rpsL*::*cat* were digested with BamH1. The digested products were ligated overnight at 16°C to combine the pJET-stitched fragment with the *rpsL*::*cat* resistance cassette.

The ligation product was transformed into Max Efficiency DH5α cells, and transformants were selected on chloramphenicol-containing LB agar plates (15 µg/mL). Colony PCR and plasmid preparations were performed to confirm the presence of the insert. For *C. jejuni* cell preparation, cultures were grown microaerobically (5% O_2, 10% CO_2, 85% N_2) at 37°C on Mueller-Hinton (MH) agar supplemented with 10% sheep blood. The verified pJET-stitched fragment containing the *rpsL*::*cat* resistance cassette was then electroporated into prepared *C. jejuni* cells. Transformants were selected on media containing chloramphenicol (15 µg/mL) and streptomycin (100 µg/mL) and screened by colony PCR.

The resulting *C. jejuni* cells carrying the *rpsL*::*cat* resistance cassette were used to create a clean deletion mutant by transforming the original pJET-stitched fragment. Sequencing was outsourced to Plasmidsaurus, with samples prepared and shipped according to their guidelines. Sequence analysis was performed using the BLAST algorithm through NCBI. Multiple sequence alignments were conducted using Clustal Omega to ensure precise deletion boundaries. Sequencing data were analyzed and compared to the whole genome sequence of the wild-type *C. jejuni* strain, also provided by Plasmidsaurus, to ensure accuracy and consistency.

The Δ*chuBCD*::Cm mutant strain was developed to investigate the role of the chuBCD genes in heme acquisition. Despite multiple attempts, a fully clean deletion was not achieved. However, the strain exhibited chloramphenicol resistance, indicating successful integration of the resistance cassette. PCR and sequencing confirmed the insertion of the chloramphenicol

resistance gene and the complete deletion of the *chuBCD* genes, validating the intended genetic modification.

Bacterial Culture and Growth Conditions. The *Campylobacter jejuni* 81-176 strain DRH212 was stored at -80°C in Mueller-Hinton broth supplemented with 20% glycerol to maintain cell viability. For this study, the *chu* genes were rendered as nonpolar deletions and constructed as plasmid-borne in the wild-type *C. jejuni* DRH212 background using previously described methods. All *C. jejuni* strains were routinely cultured on selective medium plates containing 10% sheep's blood, cefoperazone (40 μg/mL), cycloheximide (100 μg/mL), trimethoprim (10 μg/mL), and vancomycin (100 μg/mL). Cultures were incubated at 37°C under microaerobic conditions (85% N_2, 10% CO_2, and 5% O_2) for 24-72 hours. *Escherichia coli* strains used in this study were stored at -80°C in Luria-Bertani (LB) broth supplemented with 20% glycerol. These strains were grown up in a shaking incubator at 37°C in LB broth for plasmid purification and other experimental purposes. Ampicillin was added to the LB broth at a final concentration of 100 μg/mL for plasmid selection.

Heme Growth Assay. Wild-type *Campylobacter jejuni* and Δ*chu* mutants were cultured on *Campylobacter*-selective agar for 24 hours. For the growth assay, bacterial cultures were prepared in a 96-well plate format under three conditions: Mueller-Hinton broth with trimethoprim (5 μL), Mueller-Hinton broth with 100 μM hemin (dissolved in DMSO), and Mueller-Hinton broth with 100 μM hemin, 40 μM deferoxamine mesylate (DFOM), and 5 μL trimethoprim. Plates were incubated overnight at 37°C under microaerophilic conditions, and bacterial growth was quantified by measuring OD600. Visual inspection of turbidity was also performed to rule out contamination. Each experiment was conducted in triplicate and repeated at least three times to ensure reproducibility.

^{57}Fe Growth Experiments. An overnight culture was initiated in 5 mL of media. For all *Campylobacter jejuni* strains, a plate culture was started several days in advance to ensure sufficient growth. Clear tubes and 15 mL conical tubes were labeled according to experimental needs. Each clear tube was filled with 5 mL of media, while 15 mL conical tubes were prepared with 1 mL of 50% nitric acid. A 100 µM ^{57}Fe (III) Protoporphyrin IX chloride (Fisher Specialty Chemicals, Cat. # P40080) solution was prepared same day, by dissolving ^{57}Fe (III) Protoporphyrin IX chloride in dimethyl sulfoxide (DMSO). The stock was then wrapped in foil to prevent UV exposure The deferoxamine mesylate (DFOM) (Sigma-Aldrich, Cat. # 252750) solution was prepared by dissolving DFOM in ddH_2O and filtered using a 0.2 µm filter. All necessary materials, including 50% nitric acid, non-sterile water, agar plates, 96-deep well plates, sterile 1× PBS, and sterile beads, were gathered prior to the experiment.

The overnight culture's optical density (OD) at 600 nm was measured, and the culture was normalized to an OD of 0.01. Four groups were made in triplicate: MH + 10µM DFOM + 100 µM ^{57}Fe, MH + 100µM ^{57}Fe, MH only, MH + 10 10µM DFOM. *C. jejuni* strains were then added to the tubes and were incubated microaerobically at 37°C until further OD measurements were required. For cell harvesting, 100 µL of culture was transferred to the first well of the corresponding dilution plate. Cells were pelleted by centrifugation at 4000 rpm for 8 minutes, and the supernatant was discarded. The pellet was resuspended in water and centrifuged twice to ensure thorough washing. The final pellet was resuspended in 500 µL of water, weighed, and recorded. This suspension was added to a 15 mL conical tube containing 1 mL of 50% nitric acid and incubated overnight at 50°C on a heat block. The following day, 9 mL of water was added to the tube, and the sample was sent off to Vanderbilt University for ICP-MS analysis. For plating, cell suspensions were serially diluted to a final concentration of 10^{-8}. A 100 µL aliquot of the

chosen dilutions was spread onto agar plates using sterile beads. Plates were incubated at 37°C for 48-72 hours. Colony counts were performed on plates containing 30-300 colonies to ensure accurate quantification.

Mouse Infection. All animal experiments were conducted in compliance with the Institutional Animal Care and Use Committee (IACUC) guidelines at the University of Tennessee–Knoxville (UTK IACUC protocol #2885). Prior to inoculation, *C. jejuni* and Δ*chu* mutant strains were cultured onto *Campylobacter*-specific medium with 10% sheep's blood. The following day, the small amount of growth was passed onto an additional plate, creating a lawn of bacteria to ensure adequate number of cells. Prior to the infection, the cells are Gram-stained to confirm purity. Bacterial suspensions were prepared in sterile phosphate-buffered saline (PBS) and adjusted to an optical density at 600 nm (OD_{600}) of 10.

A total of 43 female-specific pathogen-free IL-10−/− C57BL/6 mice (8 to 12 weeks old) were orally gavaged with an OD of 10 *C. jejuni* wild-type strain 81-176 or Δ*chu* mutant strains. An additional seven female mice were mock-infected with the same volume of sterile 1× PBS as controls. All mice were separated into grouped cages to prevent cross-contamination and housed in the immunocompromised suite. Fecal samples (~20 mg) were collected every two days for 10 days, weighed, and diluted 1:100 in PBS. The remaining samples were immediately frozen at -80°C. Fecal samples were serially diluted in 1x PBS up to 10^{-8}, and 100 µL of each dilution was plated on *Campylobacter*-specific medium. Plates were incubated at 37°C under microaerophilic conditions for 72 hours to determine *Campylobacter* CFUs.

At the end of the 10-day infection period, blood was collected via cardiac stick, and mice were euthanized via isoflurane overdose. Secondary cervical dislocation followed as a secondary euthanasia measure. Serum was separated from the blood and stored at -20°C for further

analysis. Ceca and colons were dissected, washed five times in sterile 1× PBS, and portions were stored in 10% buffered formalin for histological analysis. Bacterial loads in tissues were quantified by weighing the organ, homogenizing the tissue, and diluting 1:100 in PBS. Serial dilutions were prepared up to 10^{-8}, and 100 µL of each dilution was plated on *Campylobacter*-selective medium. Plates were incubated for 72 hours to allow colony growth for enumeration.

Histology and Slide Preparation. Pathological scoring of intestinal tissues was performed as previously described. The terminal 1 cm of the murine colon and cecum was excised post-euthanasia, and the organ was washed five times with 1 mL of sterile, cold 1× PBS. Tissues were fixed in 10% buffered formalin for 4 hours at room temperature, embedded in paraffin, and sectioned into 4 µm slices. Sections were stained with hematoxylin and eosin (H&E) and visualized using bright-field microscopy. Representative images were captured, and inflammation scoring was conducted in a blinded manner. Scoring criteria included edema, hyperplasia, and loss of goblet cells. ImageJ and QuPath software were used to measure and quantify these criteria. ImageJ Analysis: The digital images of the tissue sections were analyzed using ImageJ. The following parameters were quantified: Edema was assessed by measuring the interstitial space within the tissue sections. ImageJ's area measurement tool was used to quantify the extent of edema, expressed in micrometers (µm). Five measurements were taken for each sample, and the average was calculated. The number of goblet cells was quantified using ImageJ's cell counting feature. Goblet cells were identified based on their distinct morphology and staining characteristics, and the total count was recorded for each tissue section. Hyperplasia was measured by examining the height of the intestinal epithelium from the base of the IEC. Hyperplasia was measured in micrometers (µm) using ImageJ's line measurement tool. Multiple measurements were taken across each tissue section, and the average thickness was calculated.

All measurements were recorded and compiled into a comprehensive dataset. For each sample, the following information was documented: Slide ID, Strain, Tissue Type (cecum or colon), Edema Measurement, Goblet Cell Count, and Hyperplasia Measurement.

Heme, Biliverdin, and Bilirubin extraction. Residual human fecal samples from standard-of-care testing were obtained from the University of Nebraska Medical Center's Department of Pathology and Microbiology (approval UTK IRB-17-03795-XM). Fecal pellets were suspended in PBS. Heme, biliverdin, and bilirubin were extracted thrice with a volume of 1 N acetic acid in ethyl acetate equal to the volume of PBS. The fecal pellet was dispersed and exposed to organic solvent through extensive vortexing. Organic/aqueous solvent phase separation was expedited by tabletop centrifugation at 4000 rpm and 4°C for 10 min. The ethyl acetate layers were transferred to clean glass tubes, combined, and dried to completion under a stream of nitrogen gas. Each sample was dissolved in 100 µL of methanol for LC-MS/MS analysis. A standard mixture of heme, biliverdin, and bilirubin was prepared in methanol at 1, 0.1, and 0.01 µM to serve as an external calibration line for quantification.

LC-MS/MS analysis. The samples were analyzed at the LSU School of Veterinary Medicine Mass Spectrometry Resource Center on a Shimadzu 8060NX triple quadrupole mass spectrometer interfaced with a Shimadzu Nexera XS 40 series UHPLC and Shimadzu CTO-40S column oven. 5 µL of each sample, blank, or standard mixture was analyzed in positive ionization mode. Chromatographic separation was achieved using a Shimadzu Nexcol C 18 (50 mm length, 2.1 mm internal diameter, 1.8 µm particle size) column with a Phenomenex Security Guard C 18 (2.1 mm internal diameter) guard column. Mobile phase A was 0.1 % formic acid in water and mobile phase B was 0.1 % formic acid in acetonitrile. The column oven was set to 25 °C and the flow rate was set to 0.4 mL/min for the entire analysis. The starting condition was 40

% B, which was held for 1 min. The B mobile phase was then ramped to 98 % over the next 14 min. The column was washed at 98 % B for 5 min, then equilibrated to 40 % B for 5 min. All instrument voltages were determined and optimized empirically prior to the analysis. The m/z transitions were 616.3 to 557.3 for heme, 583.2 to 297.2 for biliverdin, and 585.2 to 299.2 for bilirubin. An external calibration line of heme, biliverdin, and bilirubin was used to quantify each sample before normalizing to total fecal pellet weight to account for differences in the amount of starting sample.

HCT116 Cell Preparation. HCT116 cells (passage number <20) were retrieved from freezer stocks stored at -140°C to maintain cell integrity. All cell culture manipulations were performed in a sterile cell culture hood. Prior to use, all instruments and surfaces were sterilized with 70% ethanol and exposed to UV light for 15 minutes to ensure sterility. Cells were thawed and immediately transferred into a culture flask containing pre-warmed Dulbecco's Modified Eagle Medium (DMEM) (Sigma-Aldrich, Cat. # D6429) supplemented with 10% fetal bovine serum (FBS), 1% L-glutamine, and 1% penicillin-streptomycin. Cell integrity and viability were assessed under a microscope. Cultures were incubated in a humidified atmosphere at 37°C with 5% CO_2.

Cells were monitored daily, and the medium was renewed every 2-3 days to prevent nutrient depletion and accumulation of metabolic waste. Cells were passed every 2-3 days to avoid over-confluency. For passage, 0.25% Trypsin-EDTA, phenol red solution (ThermoFisher Scientific, Cat. # 25200056) was thawed to room temperature and pre-warmed to 37°C. 3 mL's of 0.25% Trypsin-EDTA were added to the flask, and the cells were incubated at 37°C for approximately 2 minutes to detach them from the flask surface. DMEM containing 10% FBS was added to inactivate the trypsin. The cell suspension was transferred to a sterile 15 mL

conical tube and centrifuged at 300 × g for 5 minutes to pellet the cells. The supernatant was carefully aspirated, and the cells were resuspended in fresh DMEM, and cell counts were performed using a hemocytometer, and an appropriate number of cells were seeded into new culture flasks for further growth.

Motility Assay. *Campylobacter jejuni* DRH212 81-176 and Δ*chu* mutants were streaked on Campylobacter-selective agar and incubated for 24 hours. *Salmonella Enterica serovar Typhimurium* was grown up on Mueller-Hinton agar plates and were grown alongside *C. jejuni* in the same microaerobic conditions. Bacterial growth was measured using a spectrophotometer at OD_{600} = 0.1. Using an autoclaved pipette tip, 1-6 µL of each bacterial suspension was stabbed into motility plates in triplicate. Plates were incubated under microaerophilic conditions at 37°C and motility measurements were recorded at 24-hour and 48-hour time points. Using a ruler, measurements were collected and analyzed using Prism10 software.

RT-qPCR analysis of gene expression. For extracting tissue and fecal RNA, RNA was extracted using a Qiagen Rneasy Kit per the manufacturer protocol. RNA samples were eluted from the kit columns using nuclease-free water and stored at -20°C. All RNA samples were then Dnase treated, and pure RNA was clean and concentrated using a kit (Zymo). Each sample was tested for DNA contamination through standard PCR. cDNA was then produced from DNA-clear RNA using the BioRad iScript kit using the manufacturer protocol. Primers specific to *rpoA* and *chuA* were designed using PrimerQuest (IDT) (Table 1). The abundance of each gene expression was determined using the iTaq Universal SYBR green master mix (BioRad). Threshold values (C_T) were used to calculate the $\Delta\Delta C_T$ using *rpoA* as the internal control for *C. jejuni* genes.

Results

In a previous study, insertion mutants of the ChuABCD transport system were examined for growth under iron-restricted conditions where heme was added as an alternative iron source. Only the mutant of ChuA was significantly affected for growth. To confirm these early results, non-polar deletion mutants were constructed and examined for growth under iron-restricted conditions where heme was added as a source of iron. After 48 hours of growth, in the absence of heme and under iron-restricted conditions, our data showed that all strains exhibited a significant ($p<0.05$) reduction in growth when compared to iron-replete conditions without added heme: wild-type (7.291667 %), Δ*chuA* (0.627614 %), Δ*chuB* (7.88957 %), Δ*chuC* (12.2331 %), Δ*chuD* (7.35992 %), and Δ*chuBCD* (16.4515 %) (**Figure 2A**). When heme was added to similar iron-restricted cultures and compared to iron-replete cultures, we found that wild-type, Δ*chuB*, Δ*chuC*, Δ*chuD*, and Δ*chuBCD*::Cm growth were restored with relative iron-replete values of 117.053%, 90.206%, 87.006%, 99.888%, and 102.578%, respectively (Figure 2A). The results from each mutant were not significantly different than the heme-dependent growth restoration that was observed for wild type *C. jejuni.* In contrast, the addition of heme was unable to restore growth for Δ*chuA* with a relative iron-replete value of only 5.017%; this result was significantly reduced ($p<0.05$) when compared to wild-type growth restoration and indicates that ChuA is a dominant determinant in the uptake and utilization of heme under iron-restricted conditions.

To further verify the role of each determinant in heme uptake, each deletion mutant under similar iron-restricted conditions but used ^{57}Fe-heme to restore growth and measured the amount of cell-associated 57Fe for each strain. Using ICP-MS to quantify the amount of cell-associated 57Fe for each strain under these conditions and found that only Δ*chuA* exhibited a significant ($p<0.05$) decrease when compared to wild-type *C. jejuni* with an average concentration of 6.9%

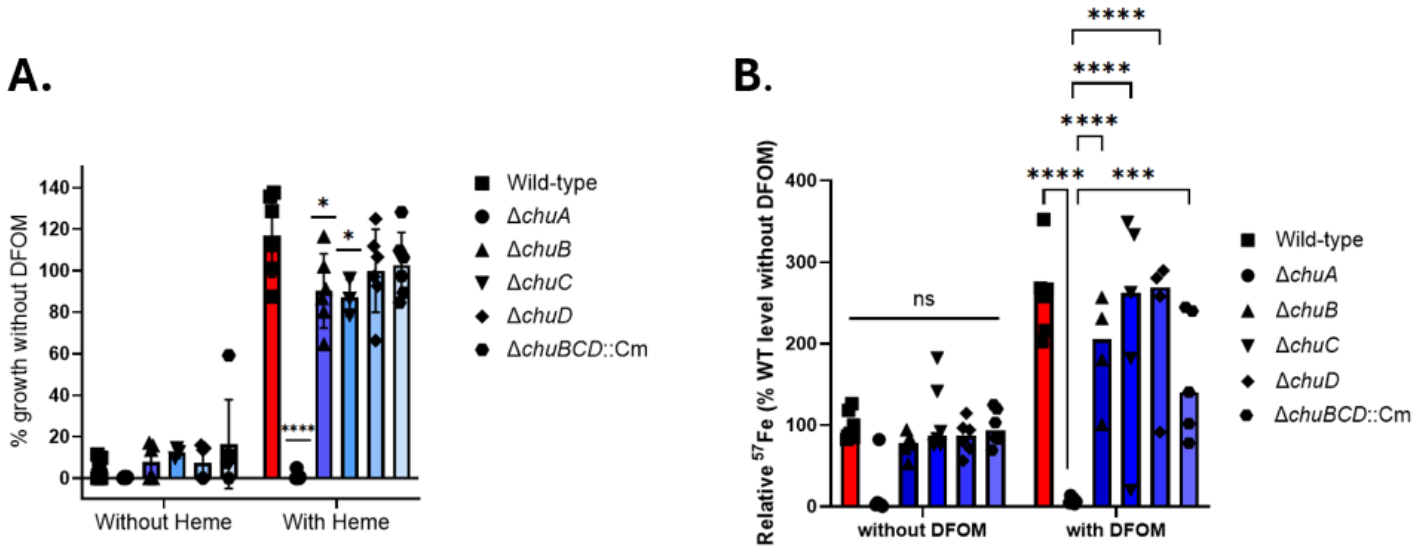

Figure 2: Mutant Growth Severely Impacted When Heme is the Sole Iron Source. (A) Growth of wild type and mutant strains *(*Δ*chuA*, Δ*chuB*, Δ*chuC,* Δ*chuD, and* Δ*chuBCD*::Cm) in the absence of deferoxamine (DFOM), with and without heme supplementation. Growth is expressed as a percentage relative to the wild-type strain. (B) Relative ^{57}Fe levels (% of wild-type without DFOM) in wild-type and mutant strains under conditions with and without DFOM. Statistical test performed was a 2-way ANOVA with Tukey's multiple comparisons Statistical significance is indicated as ****p < 0.0001, ***p<0.001, **p<0.01 and *p < 0.05. Figure made using Prism10.

versus 260.6% (**Figure 2B**). This result not only supports the earlier conclusion that ChuA is involved in acquiring iron from heme under iron-limited conditions, but because it was observed that a significant increase in ^{57}Fe under iron restriction in wild-type *C. jejuni*, the Chu system is likely induced during iron restriction. As a control, ^{57}Fe-heme was added to MH media and examined growth and the accompanying cell-associated ^{57}Fe levels. From this analysis, it was determined that only Δ*chuD* had a significant ($p<0.05$) decrease in CFUs ($9.1x10^{-2}$) when compared to wild-type *C. jejuni*. Because this was similar to the effect observed in MH media alone, it was concluded that this strain has a slight general growth defect compared to wild-type *C. jejuni*. When ^{57}Fe levels were quantified using ICP-MS, it was found that only Δ*chuA* exhibited a significant ($p<0.05$) reduction when comparing to wild-type *C. jejuni*, with average concentrations of 15.69% and 100%, respectively (**Figure. 2B**). This supports the above result that only ChuA is involved in the *in vitro* acquisition of iron from heme and that the Chu system is likely expressed at a basal level under iron-replete conditions since strains containing ChuA still secured significant amounts of ^{57}Fe from heme.

To determine how each component of the heme transport system affects *C. jejuni* infection, each of the deletion mutants was used to orally inoculate IL-10-/- mice that are susceptible to colonization and *C. jejuni*-induced gastrointestinal inflammation (**Figure 3**). Feces were collected every two days up to 10 days when the animals were euthanized and tissues harvested. At 10 days post-infection (p.i.), wild type *C. jejuni* exhibited the highest cecal colonization, with a mean of 1.93×10^7 CFU/g of tissue. By comparison, mutant strains showed significantly reduced colonization ($p < 0.05$). The Δ*chuA* mutant colonized at 5.86×10^6 CFU/g, representing a log-transformed mean difference of -0.519 compared to the wild-type. Δ*chuB* colonized at 3.72×10^5 CFU/g (-1.716 log difference), Δ*chuC* at 2.88×10^5 CFU/g (-1.826 log

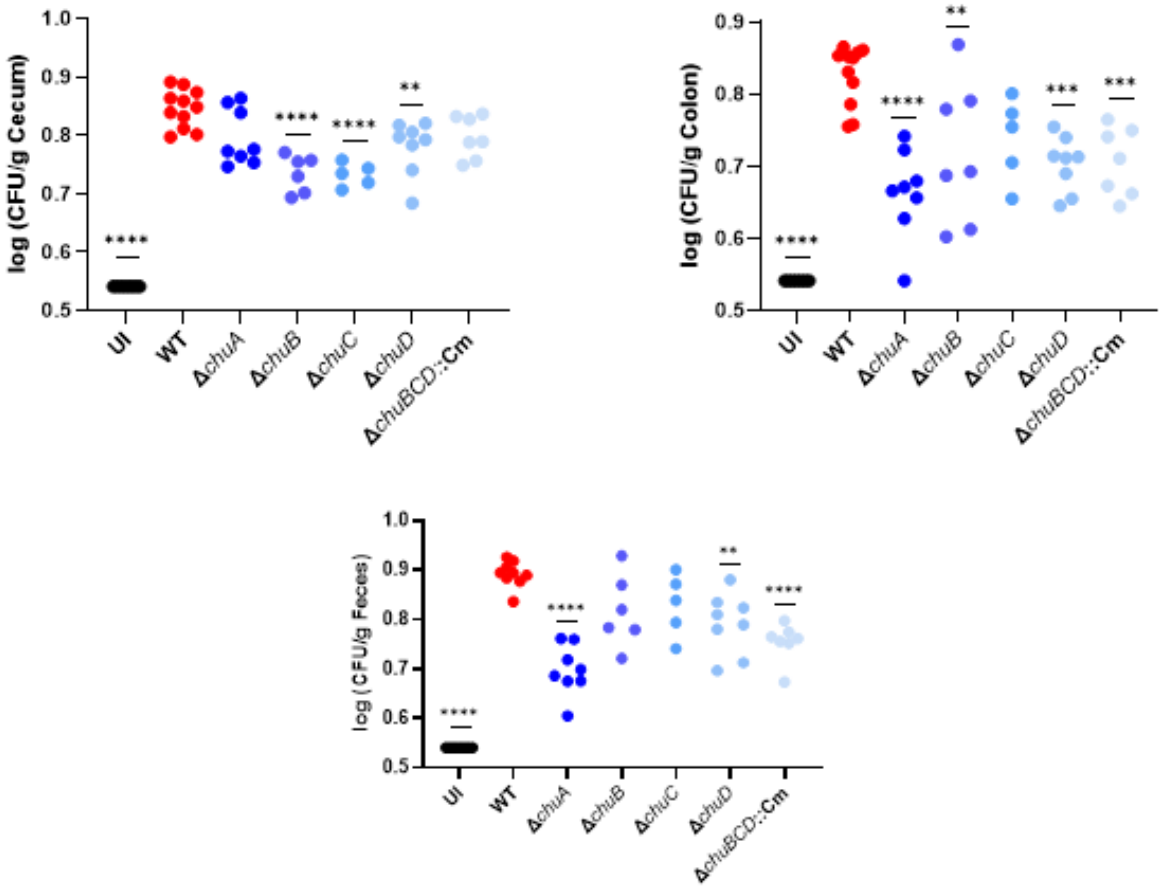

Figure 3: Colonization of *C. jejuni* wild-type and *chu* mutant strains in different intestinal compartments of IL-10 deficient mice. Bacterial loads in cecum tissue, colon tissue, and fecal samples expressed as log(CFU/g). Wild-type (WT) *C. jejuni* (red dots) showed significantly higher colonization compared to uninfected (UI) controls (black dots) across all sites. Mutant strains Δ*chuA,* Δ*chuB,* Δ*chuC,* Δ*chuD*, and Δ*chuBCD*::Cm (blue dots of varying shades) demonstrated reduced colonization compared to WT. Statistical significance was determined using one-way ANOVA with significance levels indicated as follows: **p<0.01, ***p<0.001, ****p<0.0001. Data points represent individual mice (n=5-11). Figure made using Prism10.

difference), Δ*chuD* at 1.92×10^6 CFU/g (-1.004 log difference), and Δ*chuBCD*::Cm at 3.25×10^6 CFU/g (-0.775 log difference). Interestingly, the Δ*chuA* mutant colonized the cecum at a higher rate.

To determine how each component of the heme transport system affects *C. jejuni* infection, each of the deletion mutants was used to orally inoculate IL-10-/- mice that are susceptible to colonization and *C. jejuni*-induced gastrointestinal inflammation. Feces were collected every two days up to 10 days when the animals were euthanized and tissues harvested. At 10 days post-infection (p.i.), wild type *C. jejuni* exhibited the highest cecal colonization, with a mean of 1.93×10^7 CFU/g of tissue. By comparison, mutant strains showed significantly reduced colonization ($p < 0.05$). The Δ*chuA* mutant colonized at 5.86×10^6 CFU/g, representing a log-transformed mean difference of -0.519 compared to the wild-type. Δ*chuB* colonized at 3.72×10^5 CFU/g (-1.716 log difference), Δ*chuC* at 2.88×10^5 CFU/g (-1.826 log difference), Δ*chuD* at 1.92×10^6 CFU/g (-1.004 log difference), and Δ*chuBCD*::Cm at 3.25×10^6 CFU/g (-0.775 log difference). Interestingly, the Δ*chuA* mutant colonized the cecum at a higher rate.

In the colon, wild-type *C. jejuni* colonized at 9.72×10^6 CFU/g. Mutant strains showed significant reductions in colonization ($p < 0.05$). Δ*chuA* colonized at 9.06×10^4 CFU/g (-2.0sve log difference), Δ*chuB* at 3.91×10^6 CFU/g (-0.395 log difference), Δ*chuC* at 7.14×10^5 CFU/g (-1.134 log difference), Δ*chuD* at 1.71×10^5 CFU/g (-1.755 log difference), and Δ*chuBCD*::Cm at 2.36×10^5 CFU/g (-1.614 log difference).

Fecal samples revealed the highest colonization levels for the wild-type strain, with a mean of 6.55×10^7 CFU/g. Mutant strains showed variable reductions in colonization. Δ*chuA* colonized at 2.02×10^5 CFU/g (-2.510 log difference), Δ*chuB* at 5.63×10^7 CFU/g (-0.065 log difference), Δ*chuC* at 2.54×10^7 CFU/g (-0.412 log difference), Δ*chuD* at 7.00×10^6 CFU/g (-0.971 log difference), and Δ*chuBCD*::Cm at 7.15×10^5 CFU/g (-1.962 log difference).

Analysis of *chu* gene expression across different gastrointestinal compartments, using *rpoA* as the housekeeping gene, revealed significant compartment-specific regulation. The *chuA* gene showed approximately 3-fold higher expression in the colon compared to the cecum ($p = 0.0022$), suggesting enhanced requirement for heme acquisition in this environment (**Figure 4**). This upregulation in the colon aligns with the colonization defects observed in Δ*chuA* mutant strains. Interestingly, *chuA* expression in the chyme was similar to cecal levels, but fecal samples showed intermediate expression levels that were significantly higher than chyme ($p = 0.0260$).

The observed compartment-specific regulation of *chu* expression likely reflects its critical role in shaping gut microbiota interactions and maintaining host health. Elevated *chu* expression in the colon may enhance bacterial heme acquisition, potentially influencing the competitive dynamics of gut-associated bacteria and favoring colonization by *chu*-expressing strains. This could have downstream effects on the host, including modulation of iron availability and inflammatory responses. Variations in *chu* expression may also contribute to the pathogenicity of gut-associated bacteria, as increased heme acquisition could support bacterial growth and virulence in nutrient-limited environments.

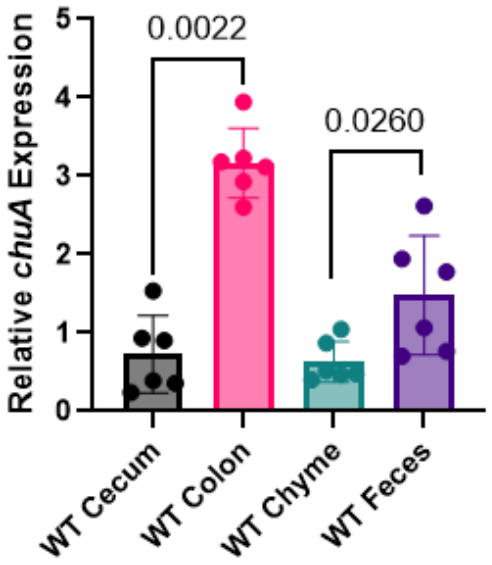

Figure 4: Relative expression of chuA in wild-type *C. jejuni* across different intestinal compartments and feces. Quantitative PCR analysis shows differential *chuA* expression levels in cecum, colon, chyme, and feces of infected mice. Expression in the colon was significantly higher compared to the cecum (p=0.0022), and fecal samples showed significantly elevated expression compared to chyme (p=0.0260). Data are presented as mean ± SEM with individual data points shown (n=6 per group). Statistical significance was determined using one-way ANOVA with p-values indicated above the relevant comparisons. Figure made using Prism10.

This study investigated the relationship between *C. jejuni* infection and fecal heme levels by analyzing stool samples from patients with and without Campylobacteriosis. The experiment aimed to determine whether *C. jejuni* infection leads to elevated heme levels in the gastrointestinal tract, potentially reflecting intestinal damage or bleeding caused by the pathogen (**Figure 5**).

The results demonstrated that patients infected with *C. jejuni* exhibited significantly higher fecal heme levels compared to uninfected individuals ($p < 0.0001$). This finding suggests that *C. jejuni* infection is associated with increased intestinal heme release, likely due to mucosal damage or hemorrhage. These elevated heme levels support the idea that heme provides a critical

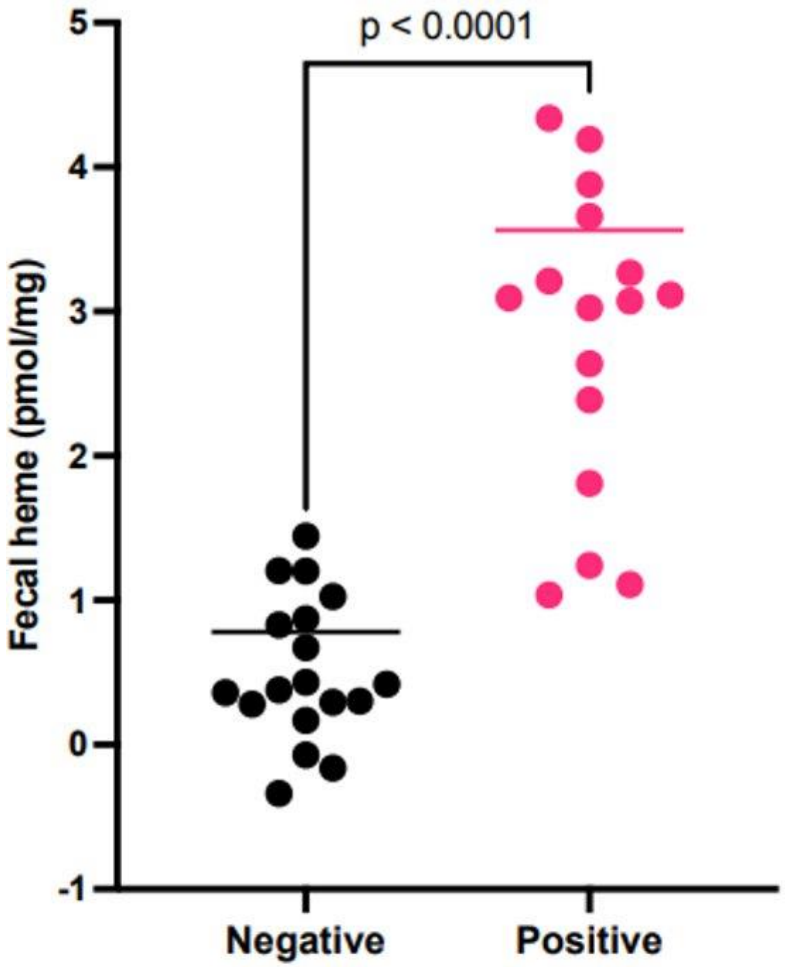

Figure 5: Human Heme Levels are elevated in *C. jejuni* infected stool. Human hospital stool samples were sent out for fecal heme quantification via HLCP. The positive samples were from patients who had been diagnosed with Campylobacteriosis (red). The negative samples were from patients who did not have Campylobacteriosis (black). The statistical test used was the Mann-Whitney U test, measured. *$p < .1$*$p < .01$; ***$p < .001$; ****$p < .0001$.

iron source for the pathogen, supporting its growth and colonization in the nutrient-limited environment of the gastrointestinal tract.

One limitation of this study is the lack of detailed information on the patients' dietary habits. Diet can significantly influence fecal heme levels, as certain foods are rich in heme iron (e.g., red meat), while others can impact gut health and mucosal integrity. Without controlling for or accounting for dietary variables, it is challenging to isolate the effect of *C. jejuni* infection on fecal heme levels from the potential confounding influence of diet.

Overall, the findings highlight the role of heme metabolism in *C. jejuni* pathogenesis and suggest that elevated fecal heme levels could serve as a marker of infection. Furthermore, the results from human samples established a found method for quantifying heme from stool samples. The experimental results also allowed for exploration of mouse fecal heme extraction and using heme measurements as a non-invasive biomarker for estimating how much heme is present in the lumen of the colon during *C. jejuni* infection. However, the results serve as an indirect measure of bleeding into the colon, but intracellular heme levels will need a more advanced mechanism to accurately measure humans and mice.

The fecal metabolite analysis revealed distinct patterns across bacterial strains, with significant differences observed in heme B, biliverdin, and bilirubin levels (**Figure 6**). Heme B levels were largely unchanged across most mutants compared to the wildtype (WT). The Δ*chuD* mutant, however, exhibited a modest but statistically significant decrease in heme B levels (mean difference = -0.1613, $p < 0.05$), while other mutant strains, including Δ*chuA* (mean difference = -0.1252, $p > 0.05$) and Δ*chuB* (mean difference = 0.2404, $p > 0.05$), showed no significant changes.

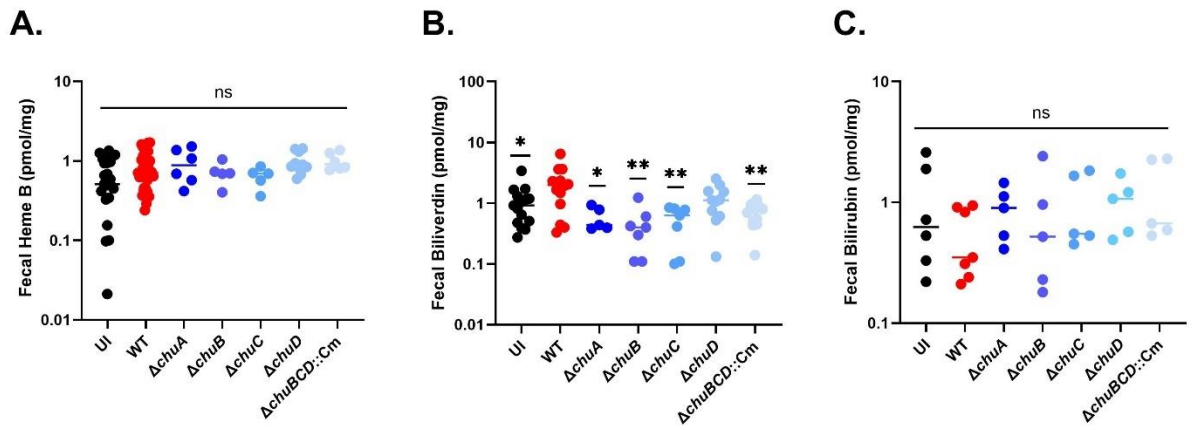

Figure 6: Biliverdin Levels Suggests Impaired Heme Metabolism. Fecal metabolite levels in uninfected (UI), wild type (WT), and various *chu* mutant strains. *(A)* Fecal heme B levels (pmol/mg), (B) fecal biliverdin levels (pmol/mg), and (C) fecal bilirubin levels (pmol/mg) were quantified using HPLC. Each dot represents an individual fecal sample. Statistical analysis was performed using one-way ANOVA with Tukey multiple comparisons. Significant differences are indicated as *$p < 0.05$ and **$p < 0.01$, while "ns" denotes non-significant differences. Unmarked comparisons indicate no significant differences. Data are presented on a log scale. Figure made using Prism10.

Biliverdin levels demonstrated more pronounced differences. The Δ*chuA* mutant exhibited a significant increase compared to wild type (mean difference = 0.3252, $p < 0.01$), while the Δ*chuD* mutant showed the highest elevation (mean difference = 0.4231, $p < 0.001$). Other mutants, such as Δ*chuB* (mean difference = 0.1123, $p > 0.05$) and Δ*chuC* (mean difference = 0.0943, $p > 0.05$), remained comparable to wild type. The Δ*chuBCD*::Cm strain displayed a moderate but significant increase in biliverdin levels (mean difference = 0.2134, $p < 0.05$).

Bilirubin levels followed a similar trend, with significant elevations observed in the Δ*chuA* (mean difference = 0.2891, $p < 0.05$) and Δ*chuD* (mean difference = 0.3567, $p < 0.001$) mutants. The Δ*chuBCD*::Cm strain also showed a moderate increase (mean difference = 0.1987, $p < 0.05$). In contrast, the Δ*chuB* (mean difference = 0.1034, $p > 0.05$) and Δ*chuC* (mean difference = 0.0876, $p > 0.05$) mutants exhibited no significant changes in bilirubin levels.

The significant differences observed in the biliverdin metabolite across bacterial strains suggest a potential role for this metabolite in strain-specific physiological or pathogenic processes. These findings indicate that biliverdin could serve as a biomarker for distinguishing bacterial strains or as a target for therapeutic interventions. Further investigation into the metabolic pathways involving biliverdin in these strains could provide insights into their unique adaptations and interactions with host environments.

Understanding the mechanisms underlying intestinal health and disease is crucial for advancing the knowledge of gastrointestinal disorders. Histopathological changes associated with edema, hyperplasia, and goblet cell loss in the mice were measured post infection to better understand how the alteration of the Chu pathway impacts the host during infection. Analysis of intestinal tissue revealed significant alterations in edema, goblet cell numbers, and hyperplasia across different experimental conditions (**Figure 7**). Edema measurements showed a marked

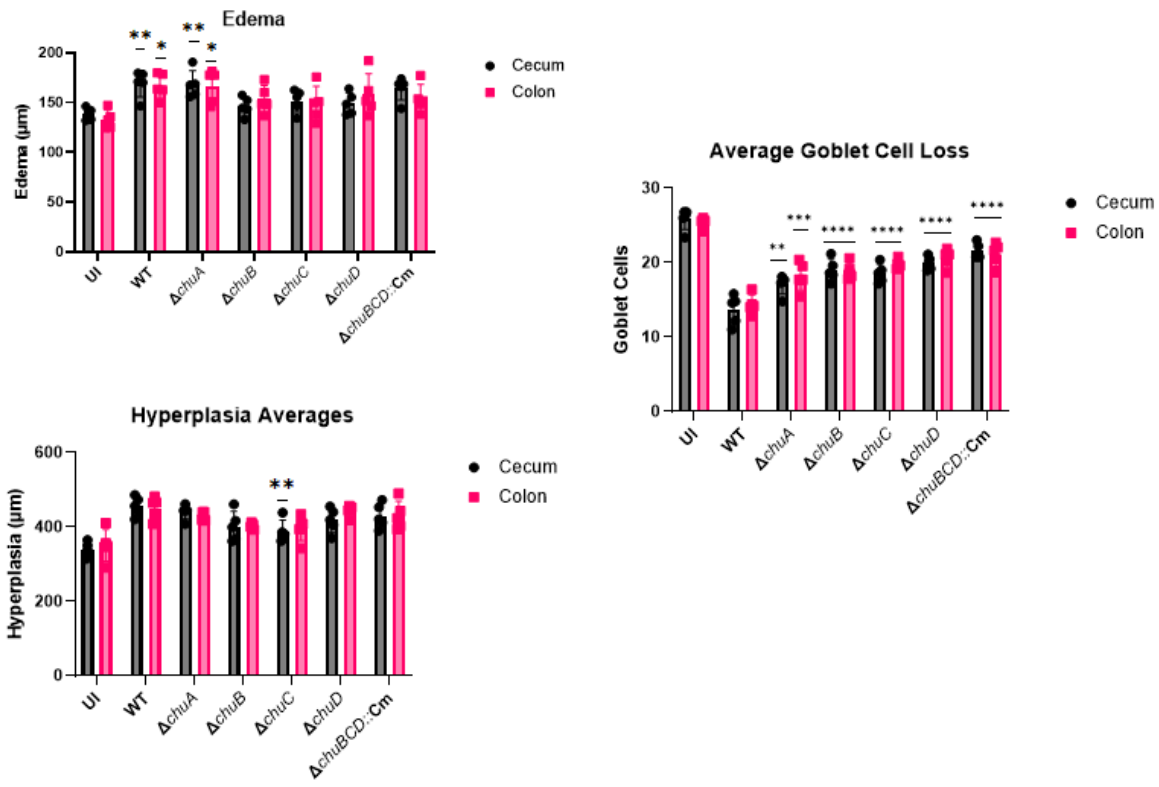

Figure 7: Histological analysis of intestinal pathology in the cecum and colon across experimental groups. (Top left) Edema measurements (µm) in the cecum and colon. (Bottom left) Hyperplasia averages (µm) in the cecum and colon. (Right) Average goblet cell loss in the cecum and colon. Each dot represents an individual sample, with black dots indicating cecum data and pink squares indicating colon data. Statistical analysis was performed using one-way ANOVA with multiple comparisons. Significant differences are denoted as *p < 0.05, **p < 0.01, ***p < 0.001, and ****p < 0.0001. Absence of statistical annotations indicates no significant differences. Figure made using Prism10.

increase in both cecum and colon tissue of WT samples compared to UI (uninfected) controls, with values reaching approximately 175-200 μm. Notably, there were significant differences ($p < 0.01$) in edema levels between cecum and colon in several experimental groups.

In the colon, edema was significantly increased in wild-type (WT) infected tissues compared to uninfected controls (-30.36, p=0.0131). The Δ*chuA* mutant strain exhibited a similar increase in edema (-29.51, p=0.0174), while other *chu* mutant strains, including Δ*chuB*, Δ*chuC*, and Δ*chuD*, showed no significant differences (p>0.05). The Δ*chuBCD*::Cm displayed a trend toward increased edema (-25.38, p=0.0625), though this did not reach statistical significance. These findings suggest that ChuA plays a critical role in mediating edema in the colon.

Hyperplasia in the colon was most pronounced in WT-infected tissues (-117.6, p<0.0001), with the Δ*chuA* mutant showing comparable effects (-102.3, p<0.0001). Δ*chuB* exhibited moderate hyperplasia (-63.21, p=0.0235), while Δ*chuC* showed a significant change (-50.46, p=0.001) in reduced hyperplasia within the cecum. The Δ*chuD* mutant demonstrated strong hyperplasia (-79.64, p=0.0013), and the Δ*chuBCD*::Cm maintained substantial hyperplastic changes (-91.36, p=0.0001). These results indicate that while ChuA is a key driver of hyperplasia, other Chu components also contribute to this phenotype.

Goblet cell loss in the colon was severe across all strains, with WT infection inducing the most significant loss (12.2, p<0.0001). The Δ*chuA* mutant also showed substantial goblet cell loss (8.8, p<0.0001), followed by Δ*chuC* (7.32, p<0.0001) and Δ*chuB* (6.88, p<0.0001). The Δ*chuD* mutant exhibited moderate loss (5.912, p<0.0001), while the Δ*chuBCD*::Cm showed the least severe but still significant loss (4.276, p<0.0001). These findings highlight the hierarchical importance of Chu components in maintaining goblet cell integrity.

Chapter III

Discussion

The role of heme in campylobacteriosis is poorly understood. The upregulation of *chu* genes in during human infections indicates that heme-iron sources play a critical role in successful colonization and in turn, a greater disease state in humans. Supporting earlier findings, it was observed that ChuA is the sole protein required for growth when heme is provided as an alternative iron source under iron-restricted conditions (**Figure 2A**). Individual mutant strains of the predicted inner membrane transporter exhibited growth levels comparable to the wild type under these conditions. Further analysis using isotopically labeled heme (^{57}Fe) revealed that ChuA is the only determinant necessary for acquiring iron from heme (**Figure 2B**). This experiment also demonstrated that the acquisition of heme-derived iron increases under iron-restricted conditions, aligning with gene expression studies that show elevated *chuZABCD* transcript levels under low iron availability, regulated by the ferric uptake regulator (Fur). Interestingly, ChuA-dependent acquisition of heme-derived iron was detectable even under iron-replete conditions, suggesting a baseline level of constitutive Chu expression.

The hypothesis of functional redundancy for ChuBCD in the genome was initially proposed, supported by the absence of a ChuA homolog in the *C. jejuni* 81-176 genome. Additionally, CeuB, the ABC-type enterochelin permease, shares 30% amino acid identity and 50% positive residues with ChuB, while CeuD, the ABC-type enterochelin ATPase, exhibits 30% amino acid identity and 58% positive residues with ChuC. Beyond CeuD, 22 additional genes encode potential ChuC homologs with 92-73% coverage and 36.97-24.31% amino acid identity. However, the absence of a ChuD homolog in the *C. jejuni* 81-176 genome challenges this redundancy hypothesis. Further research is required to determine whether components of the enterochelin transport system can functionally substitute for Chu determinants and elucidate the

mechanism by which heme-derived iron is transported into the bacterium in the absence of the periplasmic substrate-binding protein homolog.

The motility, adhesion, and invasion capabilities of *C. jejuni* represent interconnected virulence mechanisms essential for successful host colonization and pathogenesis. Previous studies have demonstrated that motility, primarily driven by flagellar function, serves as a prerequisite for efficient adhesion and subsequent invasion of host epithelial cells (26). Experimentally, it was necessary to determine that the *chu* mutant strains maintained full functionality of these systems, and that potential alterations in later experiments were due to the lack of heme, rather than these traits. Testing these fitness factors also provides a secondary confirmation that deleting *chu* genes did not make unintended downstream genetic alterations of these systems.

Motility is one of *C. jejuni's* most important virulence factors and non-motile *C. jejuni* is not able to successfully migrate the mucus layer of the gastrointestinal tract and is unable to adhere and invade the IEC's (11,84). It was determined that *chu* knockout strains exhibited similar motility compared to the wildtype (**Figure 12**). Interestingly, Δ*chuBCD*::Cm showed an increased motility phenotype. The increased motility phenotype might represent an adaptive response where *C. jejuni* compensates for reduced heme-iron acquisition capability by enhancing its ability to seek out other iron uptake systems. However, this was not observed in Δ*chuA*, which cannot utilize heme. One hypothesis is that the absence of ChuBCD triggers compensatory upregulation of alternative iron acquisition systems or an unknown inner membrane alteration to acquire heme. It is unknown how Δ*chuBCD*::Cm motility benefits or detracts from successful colonization *in vivo*. It can be hypothesized that increased mobility allows for increased fitness by allowing Δ*chuBCD*::Cm to migrate the mucus layer of the gastrointestinal tract but the overall

peak of Δ*chuBCD*::Cm was found to be during Day 6 of infection (**Figure 8**). This increased mobility may come at a cost of increased energy expenditure that Δ*chuBCD*::Cm cannot recover from long-term. More research is needed to expand on these findings.

The current findings reveal that the disruption of the Chu system does not impair these critical virulence factors, suggesting their regulation operates independently of heme-iron availability. *C. jejuni* invasion (**Figure 9**) and adherence (**Figure 10**) capabilities were comparable compared to wild type, which suggests that CadF and FlpA functionality is not altered by the lack of heme-iron (28).

The expression pattern of *chu* genes was notably higher in the colon compared to the cecum, consistent with prior literature identifying the colon as a critical niche for this pathogen (83). The colon may provide an optimal environment for heme acquisition gene expression due to its relatively stable ecological conditions and consistent nutrient availability compared to other gastrointestinal regions (85). Lower *chu* gene expression in the cecum could be the result of a combination of several factors such as dietary iron presence. Most dietary iron absorption occurs in the duodenum and the jejunum (86). This suggests that most of the dietary iron is absorbed prior to reaching the cecum or colon. However, given the closer proximity of the cecum to the duodenum and the jejunum, some dietary iron may reach the cecum, allowing *C. jejuni* to access this iron source, downregulating the expression of *chu* genes.

The enhanced expression of *chu* genes in the colon likely facilitates *C. jejuni* colonization and subsequent pathogenesis. This may be attributed to the lower iron availability in the colon's thicker mucus layer, which necessitates upregulation of *chu* genes to acquire heme-iron from the environment. As *C. jejuni* migrates deeper into the colonic mucus layers, access to luminal iron sources diminishes, increasing reliance on heme-iron found in IEC's (87,88). Additionally, to

counteract iron starvation, *C. jejuni* invades host cells to access intracellular heme, a phenomenon supported by the frequent occurrence of colonic bleeding in *C. jejuni* infections.

To address the question of whether colonization rates are affected regarding altered Chu function and *in vivo* mouse model was used. The results of *chu* colonization experiments indicate that altered Chu function significantly impacts *C. jejuni* colonization rates. Mice infected with *chu* knockout strains exhibited reduced colonization levels compared to those infected with wild-type strains (**Figure 3**), suggesting that the Chu system plays a critical role in establishing and maintaining colonization in the host. This finding aligns with the hypothesis that heme acquisition is essential for *C. jejuni* survival and persistence in the inflamed gut environment, where iron availability is limited due to host sequestration mechanisms (88–90).

Interestingly, there seems to be consistent patterns for colonization. Δ*chuA* and Δ*chuBCD*::Cm colonized the cecum comparable to wild-type but colonization was significantly reduced in the colon. This indicates that ChuA and the full operon may not be as critical in this region, possibly due to the availability of alternative iron sources or reduced reliance on heme acquisition. However, the significant reduction in colon colonization by these mutant strains highlights the importance of the Chu system in environments with more restricted iron availability. In contrast, Δ*chuB,* Δ*chuC,* and Δ*chuD* were significantly reduced in the cecum compared to other mutant strains but overall Δ*chuB* and Δ*chuC* colonized the colon more successfully. This suggests that these deletions that challenge the cells may be less severe in the context of heme acquisition. It is currently unknown if other factors, aside from iron, modulate heme-iron acquisition in the cecum and colon and warrants further investigation.

Additionally, differences in the normal microbiome between the cecum and colon may influence *C. jejuni* colonization and immune responses. The cecum typically harbors a more

diverse and dense microbial community, which could compete with *C. jejuni* for resources or modulate the immune response in ways that favor colonization. Conversely, the colon's microbiome may be less conducive to *C. jejuni* colonization, either through direct competition or by promoting a less inflammatory environment. These microbiome differences, combined with the distinct immune cell profiles, likely shape the region-specific colonization patterns observed in the *chu* deletion mutants.

The discrepancy between our observations and previous studies showing more severe tissue damage may be explained by variations in host response or environmental conditions. For instance, the severity of *C. jejuni*-induced inflammation can vary significantly depending on the host's microbiota composition and immune status. The reduced tissue damage in our study, despite normal colonization levels, suggests that additional host or environmental factors may be modulating the pathogen's virulence expression.

The similar heme levels (**Figure 5**) across strains, therefore, reflect a combination of reduced tissue damage and the complex regulation of virulence factors in *C. jejuni*. The role of ChuZ in this context appears to be secondary to the overall host tissue response, suggesting that under conditions of reduced inflammation, the heme uptake and degradation pathway may not be operating at its full capacity. Thos finding opens new questions about the environmental and host factors that influence *C. jejuni* virulence expression and subsequent tissue damage, independent of bacterial load.

The reduction in goblet cell numbers observed in the wildtype strain in our experiments, coupled with low edema and hyperplasia, raised intriguing questions about why this is occurring. One hypothesis is that dysbiosis of the normal microbiome altered mucus production. Goblet cells are essential for producing mucins, particularly MUC2, which maintain the intestinal mucus

barrier and prevent bacterial adhesion, thereby supporting gut homeostasis. However, with dysbiosis and goblet cell loss, inflammation in the form of edema can be expected (**Figure 7**). Another hypothesis is that macrophages are playing a role in regulating goblet cells within both the cecum and colon. Literature suggests that this is the case, M1 macrophages, which serve an inflammatory role, tend to suppress goblet cell differentiation and mucus production, leading to goblet cell loss. The inverse can occur with M2 macrophages, which are anti-inflammatory (65). The main cytokines that cause goblet cell control, particularly IL-9 should be quantified to address this hypothesis in the future.

These hypotheses suggest a complex interplay between microbiota, immune cells, and intestinal barrier function that warrants further investigation. Future studies should examine the temporal relationship between dysbiosis onset and goblet cell depletion, particularly focusing on whether specific bacterial populations directly influence MUC2 expression. Additionally, characterizing the M1/M2 macrophage ratio in affected tissues, along with their secreted cytokine profiles (including IL-9, IL-13, and IL-22), would help elucidate the immune mechanisms driving goblet cell dysfunction (65). The role of other immune cells, such as innate lymphoid cells (ILCs) and T helper cells, should also be considered as they are known to influence both macrophage polarization and goblet cell function. Understanding these pathways could reveal potential therapeutic targets for restoring normal barrier function, either through microbiome modulation, immune response modification, or direct enhancement of mucin production.

Future Directions

Future research on *Campylobacter jejuni* and heme acquisition should focus on elucidating alternative iron acquisition mechanisms that enable colonization in the absence of ChuA. Investigating the role of other iron transport systems, such as ferric citrate uptake or siderophore-mediated pathways, could provide insights into redundant or compensatory mechanisms. Additionally, spatial regulation of *chu* gene expression warrants further exploration, particularly in response to varying iron availability and inflammatory conditions across different gastrointestinal regions. Additional *in vivo* models should be investigated to see if *chu* colonization phenotypes are reproducible in other animal models such as ferrets. A key limitation of our current study is the single time point analysis of heme metabolites at Day 10 post-infection. While this time point represents peak *C. jejuni* colonization, it provides only a snapshot of the dynamic host-pathogen interaction. Future studies should implement daily mass spectrometry analysis of fecal samples throughout the 10-day infection period to track temporal changes in heme *b*, biliverdin, and bilirubin levels.

Additionally, the use of older IL-10 deficient mice (>6 months) could enhance our understanding of *C. jejuni* pathogenesis in the context of chronic inflammation. As these mice develop more severe intestinal inflammation with age, they may exhibit exaggerated histological changes during infection. Since the histology wasn't as severe as anticipated compared to prior laboratory experiments in the lab, this model could better reflect the inflammatory conditions observed in human campylobacteriosis and provide a more pronounced system for studying heme-dependent colonization strategies. The combination of metabolite analysis and aged IL-10 deficient mice would offer a more comprehensive view of the dynamic interplay between host inflammation, heme availability, and *C. jejuni* colonization throughout the infection cycle.

References

1. Vandamme P, Debruyne L, De Brandt E, Falsen E. Reclassification of Bacteroides ureolyticus as Campylobacter ureolyticus comb. nov., and emended description of the genus Campylobacter. Vol. 60, International Journal of Systematic and Evolutionary Microbiology. 2010. p. 2016–22.

2. Iswaran A, Okoh AI. Human campylobacteriosis: A public health concern of global importance. Vol. 5, Heliyon. Elsevier Ltd; 2019.

3. Shah HJ, Jervis RH, Wymore K, Rissman T, LaClair B, Boyle MM, et al. Morbidity and Mortality Weekly Report Reported Incidence of Infections Caused by Pathogens Transmitted Commonly Through Food: Impact of Increased Use of Culture-Independent Diagnostic Tests-Foodborne Diseases Active Surveillance Network, 1996-2023. 2024; Available from: https://www.cdc.gov/mmwr/mmwr_continuingEducation.html

4. Damborg P, Olsen KEP, Nielsen EM, Guardabassi L. Occurrence of Campylobacter jejuni in Pets Living with Human Patients Infected with C. jejuni. J Clin Microbiol. 2004 Mar;42(3):1363–4.

5. Scharff RL. Economic burden from health losses due to foodborne illness in the united states. J Food Prot. 2012 Jan;75(1):123–31.

6. Kiarie A, Bebora L, Gitao G, Ochien'g L, Okumu N, Mutisya C, et al. Prevalence and risk factors associated with the occurrence of Campylobacter sp. in children aged 6–24 months in peri-urban Nairobi, Kenya. Front Public Health. 2023;11.

7. Abay KA, Desalegn G, Weldu Y, Gebrehiwot GT, Gebreyohannes G, Welekidan LN, et al. Prevalence and Antimicrobial Resistance of Campylobacter Species and Associated Factors Among Under-Five Children with Diarrhea at Randomly Selected Public Health Facilities in Mekelle, Tigray, Ethiopia. Infect Drug Resist. 2024;17:495–505.

8. Johnson JG, Gaddy JA, DiRita VJ. The PAS domain-containing protein heur regulates heme uptake in Campylobacter jejuni. mBio. 2016 Jan 1;7(6).

9. Grant CCR, Konkel ME, Cieplak W, Tompkins1' LS. Role of Flagella in Adherence, Internalization, and Translocation of Campylobacterjejuni in Nonpolarized and Polarized Epithelial Cell Cultures [Internet]. INFECTION AND IMMUNITY. 1993. Available from: https://journals.asm.org/journal/iai

10. Motility of Campylobacter jejuni in a Viscous Environment: Comparison with Conventional Rod-shaped Bacteria. Vol. 134, Journal of General Microbiology. 1988.

11. Stahl M, Frirdich E, Vermeulen J, Badayeva Y, Li X, Vallance BA, et al. The helical shape of Campylobacter jejuni promotes in vivo pathogenesis by aiding transit through intestinal mucus and colonization of crypts. Infect Immun. 2016;84(12):3399–407.

12. Taheri N, Fällman M, Wai SN, Fahlgren A. Accumulation of virulence-associated proteins in Campylobacter jejuni Outer Membrane Vesicles at human body temperature. J Proteomics. 2019 Mar 20;195:33–40.

13. Méndez-Olvera ET, Bustos-Martínez JA, López-Vidal Y, Verdugo-Rodríguez A, Martínez-Gómez D. Cytolethal distending toxin from campylobacter jejuni requires the cytoskeleton for toxic activity. Jundishapur J Microbiol. 2016 Oct 1;9(10).

14. Callahan SM, Dolislager CG, Johnson JG. The host cellular immune response to infection by campylobacter spp. And its role in disease. Vol. 89, Infection and Immunity. American Society for Microbiology; 2021.

15. Callahan S, Doster RS, Jackson JW, Kelley BR, Gaddy JA, Johnson JG. Induction of neutrophil extracellular traps by Campylobacter jejuni. Cell Microbiol. 2020 Aug 1;22(8).

16. Tribble DR, Baqar S, Scott DA, Oplinger ML, Trespalacios F, Rollins D, et al. Assessment of the duration of protection in Campylobacter jejuni experimental infection in humans. Infect Immun. 2010 Apr;78(4):1750–9.

17. Badjo AOR, Kabore NF, Zongo A, Gnada K, Ouattara A, Muhigwa M, et al. Burden and epidemiology of Campylobacter species in acute enteritis cases in Burkina Faso. BMC Infect Dis. 2024 Dec 1;24(1).

18. Omarova S, Awad K, Moos V, Püning C, Gölz G, Schulzke JD, et al. Intestinal Barrier in Post-Campylobacter jejuni Irritable Bowel Syndrome. Biomolecules. 2023 Mar 1;13(3).

19. Tian T, Wang Z, Zhang J. Pathomechanisms of Oxidative Stress in Inflammatory Bowel Disease and Potential Antioxidant Therapies. Vol. 2017, Oxidative Medicine and Cellular Longevity. Hindawi Limited; 2017.

20. He Z, Gharaibeh RZ, Newsome RC, Pope JL, Dougherty MW, Tomkovich S, et al. Campylobacter jejuni promotes colorectal tumorigenesis through the action of cytolethal distending toxin. Gut. 2019 Feb 1;68(2):289–300.

21. Sinha R, LeVeque RM, Callahan SM, Chatterjee S, Stopnisek N, Kuipel M, et al. Gut metabolite L-lactate supports Campylobacter jejuni population expansion during acute infection. Proc Natl Acad Sci U S A. 2024;121(2).

22. Nyati KK, Nyati R. Role of campylobacter jejuni infection in the pathogenesis of Guillain-Barré syndrome: An update. Vol. 2013, BioMed Research International. 2013.

23. Mccarthy N, Giesecke J. Incidence of Guillain-Barré Syndrome following Infection with Campylobacter jejuni [Internet]. Vol. 153. 2001. Available from: https://academic.oup.com/aje/article/153/6/610/136973

24. Garg AX, Pope JE, Thiessen-Philbrook H, Clark WF, Ouimet J. Arthritis risk after acute bacterial gastroenteritis. Rheumatology. 2008;47(2):200–4.

25. Ribardo DA, Johnson JJ, Hendrixson DR. Viscosity-dependent determinants of Campylobacter jejuni impacting the velocity of flagellar motility. mBio. 2024 Jan 1;15(1).

26. Cohen EJ, Nakane D, Kabata Y, Hendrixson DR, Nishizaka T, Beeby M. Campylobacter jejuni motility integrates specialized cell shape, flagellar filament, and motor, to coordinate action of its opposed flagella. PLoS Pathog. 2020 Jul 1;16(7).

27. Gabbert AD, Mydosh JL, Talukdar PK, Gloss LM, McDermott JE, Cooper KK, et al. The Missing Pieces: The Role of Secretion Systems in Campylobacter jejuni Virulence. Vol. 13, Biomolecules. MDPI; 2023.

28. Konkel ME, Talukdar PK, Negretti NM, Klappenbach CM. Taking Control: Campylobacter jejuni Binding to Fibronectin Sets the Stage for Cellular Adherence and Invasion. Vol. 11, Frontiers in Microbiology. Frontiers Media S.A.; 2020.

29. Svensson SL, Pryjma M, Gaynor EC. Flagella-mediated adhesion and extracellular DNA release contribute to biofilm formation and stress tolerance of Campylobacter jejuni. PLoS One. 2014 Aug 28;9(8).

30. Kreling V, Falcone FH, Kehrenberg C, Hensel A. Campylobacter sp.: Pathogenicity factors and prevention methods-new molecular targets for innovative antivirulence drugs? Available from: https://doi.org/10.1007/s00253-020-10974-5

31. Neal-McKinney JM, Konkel ME. The Campylobacter jejuni CiaC virulence protein is secreted from the flagellum and delivered to the cytosol of host cells. Front Cell Infect Microbiol. 2012;2:31.

32. Harrer A, Bücker R, Boehm M, Zarzecka U, Tegtmeyer N, Sticht H, et al. Campylobacter jejuni enters gut epithelial cells and impairs intestinal barrier function through cleavage of occludin by serine protease HtrA. Gut Pathog. 2019 Feb 13;11(1).

33. Sharafutdinov I, Esmaeili DS, Harrer A, Tegtmeyer N, Sticht H, Backert S. Campylobacter jejuni Serine Protease HtrA Cleaves the Tight Junction Component Claudin-8. Front Cell Infect Microbiol. 2020 Dec 8;10.

34. Hatayama S, Shimohata T, Amano S, Kido J, Nguyen AQ, Sato Y, et al. Cellular tight junctions prevent effective Campylobacter jejuni invasion and inflammatory barrier disruption promoting bacterial invasion from lateral membrane in polarized intestinal epithelial cells. Front Cell Infect Microbiol. 2018 Jan 30;8(JAN).

35. Maini RN, Elliott MJ, Brennan FM, Feldmann M. Beneficial effects of tumour necrosis factor-alpha (TNF-α) blockade in rheumatoid arthritis (RA). Vol. 101, Clinical and Experimental Immunology. Blackwell Publishing Ltd; 1995. p. 207–12.

36. Naikare H, Palyada K, Panciera R, Marlow D, Stintzi A. Major role for FeoB in Campylobacter jejuni ferrous iron acquisition, gut colonization, and intracellular survival. Infect Immun. 2006 Oct;74(10):5433–44.

37. Van Vliet AHM, Ketley JM, Park SF, Penn CW. The role of iron in Campylobacter gene regulation, metabolism and oxidative stress defense. FEMS Microbiol Rev. 2002 Jun 1;26(2):173–86.

38. Butcher J, Handley RA, van Vliet AHM, Stintzi A. Refined analysis of the Campylobacter jejuni iron-dependent/independent Fur- and PerR-transcriptomes. BMC Genomics. 2015 Jul 4;16(1).

39. Parkhill, J., Wren, B., Mungall, K. et al. The genome sequence of the food-borne pathogen Campylobacter jejuni reveals hypervariable sequences. Nature 403, 665–668 (2000). https://doi.org/10.1038/35001088.

40. Palyada K, Threadgill D, Stintzi A. Iron acquisition and regulation in Campylobacter jejuni. J Bacteriol. 2004 Jul;186(14):4714–29.

41. Ridley KA, Rock JD, Li Y, Ketley JM. Heme utilization in Campylobacter jejuni. J Bacteriol. 2006 Nov;188(22):7862–75.

42. Oh E, Andrews KJ, Jeon B. Enhanced biofilm formation by ferrous and ferric iron through oxidative stress in Campylobacter jejuni. Front Microbiol. 2018 Jun 6;9(JUN).

43. Holmes K, Mulholland F, Pearson BM, Pin C, McNicholl-Kennedy J, Ketley JM, et al. Campylobacter jejuni gene expression in response to iron limitation and the role of Fur. Microbiology (N Y). 2005 Jan;151(1):243–57.

44. Zheng J, Meng J, Zhao S, Singh R, Song W. Campylobacter-induced interleukin-8 secretion in polarized human intestinal epithelial cells requires Campylobacter-secreted cytolethal distending toxin- and toll-like receptor-mediated activation of NF-κB. Infect Immun. 2008 Oct;76(10):4498–508.

45. Kelley BR, Callahan SM, Johnson JG. Transcription of cystathionine b-lyase (MetC) is repressed by heur in Campylobacter jejuni, and methionine biosynthesis facilitates colonocyte invasion. J Bacteriol. 2021 Aug 1;203(15).

46. Callahan SM, Hancock TJ, Doster RS, Parker CB, Wakim ME, Gaddy JA, et al. M I C R O B I O LO G Y A secreted sirtuin from Campylobacter jejuni contributes to neutrophil activation and intestinal inflammation during infection [Internet]. 2023. Available from: https://www.science.org

47. Mansfield LS, Bell JA, Wilson DL, Murphy AJ, Elsheikha HM, Rathinam VAK, et al. C57BL/6 and congenic interleukin-10-deficient mice can serve as models of Campylobacter jejuni colonization and enteritis. Infect Immun. 2007 Mar;75(3):1099–115.

48. Gill N, Ferreira RBR, Antunes LCM, Willing BP, Sekirov I, Al-Zahrani F, et al. Neutrophil Elastase Alters the Murine Gut Microbiota Resulting in Enhanced Salmonella Colonization. PLoS One. 2012 Nov 14;7(11).

49. Johansson MEV, Holmén Larsson JM, Hansson GC. The two mucus layers of colon are organized by the MUC2 mucin, whereas the outer layer is a legislator of host-microbial interactions. Proc Natl Acad Sci U S A. 2011 Mar 15;108(SUPPL. 1):4659–65.

50. Bergström A, Kristensen MB, Bahl MI, Metzdorff SB, Fink LN, Frøkiær H, et al. Nature of bacterial colonization influences transcription of mucin genes in mice during the first week of life. BMC Res Notes. 2012;5.

51. Wang Z, Shen J. The role of goblet cells in Crohn' s disease. Vol. 14, Cell and Bioscience. BioMed Central Ltd; 2024.

52. Bergstrom KSB, Kissoon-Singh V, Gibson DL, Ma C, Montero M, Sham HP, et al. Muc2 protects against lethal infectious colitis by disassociating pathogenic and commensal bacteria from the colonic mucosa. PLoS Pathog. 2010 May;6(5).

53. Chang C, Miller JF. Campylobacter jejuni colonization of mice with limited enteric flora. Infect Immun. 2006 Sep;74(9):5261–71.

54. Knippel RJ, Wexler AG, Miller JM, Beavers WN, Weiss A, de Crécy-Lagard V, et al. Clostridioides difficile Senses and Hijacks Host Heme for Incorporation into an Oxidative Stress Defense System. Cell Host Microbe. 2020 Sep 9;28(3):411-421.e6.

55. Teng Y, Luo HR, Kambara H. Heterogeneity of neutrophil spontaneous death. Vol. 92, American Journal of Hematology. Wiley-Liss Inc.; 2017. p. E156–9.

56. Hong CW. Current understanding in neutrophil differentiation and heterogeneity. Vol. 17, Immune Network. Korean Association of Immunologists; 2017. p. 298–306.

57. Mestas J, Hughes CCW. IMMUNOLOGY Of Mice and Not Men: Differences between Mouse and Human Immunology [Internet]. Vol. 172, The Journal of Immunology. 2004. Available from:http://journals.aai.org/jimmunol/article-pdf/172/5/2731/1181081/2731.pdf

58. Doeing DC, Borowicz JL, Crockett ET. BMC Clinical Pathology Gender dimorphism in differential peripheral blood leukocyte counts in mice using cardiac, tail, foot, and saphenous vein puncture methods micegender dimorphismblood collectioncardiac puncturetail veinSaphenousfoot veinleukocyte counts [Internet]. 2003. Available from: http://www.biomedcentral.com/1472-6890/3/3

59. Schneider A, Krüger C, Steigleder T, Weber D, Pitzer C, Laage R, et al. The hematopoietic factor G-CSF is a neuronal ligand that counteracts programmed cell death and drives neurogenesis. Journal of Clinical Investigation. 2005 Aug;115(8):2083–98.

60. Green SM, Vowels J, Waterman B, Rothrock SG, Kuniyoshi G. Leukocytosis: A new look at an old marker for acute myocardial infarction. Academic Emergency Medicine. 1996;3(11):1034–41.

61. Liu F, Wu Y, Wesselschmidt R. Impaired Production and Increased Apoptosis of Neutrophils in Granulocyte Colony-Stimulating Factor Receptor-Deficient Mice. Vol. 5, Immunity. 1996.

62. Lieschke GJ, Grail D, Hodgson G, Metcalf D, Stanley E, Cheers C, et al. RAPID COMMUNICATION Mice Lacking Granulocyte Colony-Stimulating Factor Have Chronic Neutropenia, Granulocyte and Macrophage Progenitor Cell Deficiency, and Impaired Neutrophil Mobilization [Internet]. Available from: http://ashpublications.org/blood/article-pdf/84/6/1737/615743/1737.pdf

63. Shank JM, Kelley BR, Jackson JW, Tweedie JL, Franklin D, Damo SM, et al. The Host Antimicrobial Protein Calgranulin C Participates in the Control of Campylobacter jejuni Growth via Zinc Sequestration. 2018; Available from: https://doi.org/10.1128/IAI

64. Palmer LJ, Cooper PR, Ling MR, Wright HJ, Huissoon A, Chapple ILC. Hypochlorous acid regulates neutrophil extracellular trap release in humans. Clin Exp Immunol. 2012 Feb;167(2):261–8.

65. Italiani P, Boraschi D. From monocytes to M1/M2 macrophages: Phenotypical vs. functional differentiation. Vol. 5, Frontiers in Immunology. Frontiers Media SA; 2014.

66. Scott CL, Zheng F, De Baetselier P, Martens L, Saeys Y, De Prijck S, et al. Bone marrow-derived monocytes give rise to self-renewing and fully differentiated Kupffer cells. Nat Commun. 2016 Jan 27;7.

67. Ginhoux F, Greter M, Leboeuf M, Nandi S, See P, Gokhan S, et al. Fate mapping analysis reveals that adult microglia derive from primitive macrophages. Science (1979). 2010 Nov 5;330(6005):841–5.

68. Schridde A, Bain CC, Mayer JU, Montgomery J, Pollet E, Denecke B, et al. Tissue-specific differentiation of colonic macrophages requires TGFβ receptor-mediated signaling. Mucosal Immunol. 2017 Nov 1;10(6):1387–99.

69. Lee M, Lee Y, Song J, Lee J, Chang SY. Tissue-specific role of CX3CR1 expressing immune cells and their relationships with human disease. Vol. 18, Immune Network. Korean Association of Immunologists; 2018.

70. Zigmond E, Varol C, Farache J, Elmaliah E, Satpathy AT, Friedlander G, et al. Ly6Chi Monocytes in the Inflamed Colon Give Rise to Proinflammatory Effector Cells and Migratory Antigen-Presenting Cells. Immunity. 2012 Dec 14;37(6):1076–90.

71. Liu XB, Nguyen NBH, Marquess KD, Yang F, Haile DJ. Regulation of hepcidin and ferroportin expression by lipopolysaccharide in splenic macrophages. Blood Cells Mol Dis. 2005 Jul 1;35(1):47–56.

72. Schaer CA, Schoedon G, Imhof A, Kurrer MO, Schaer DJ. Constitutive endocytosis of CD163 mediates hemoglobin-heme uptake and determines the noninflammatory and protective transcriptional response of macrophages to hemoglobin. Circ Res. 2006 Oct;99(9):943–50.

73. Mesquita G, Silva T, Gomes AC, Oliveira PF, Alves MG, Fernandes R, et al. H-Ferritin is essential for macrophages' capacity to store or detoxify exogenously added iron. Sci Rep. 2020 Dec 1;10(1).

74. Braun V, Ratliff AC, Celia H, Buchanan SK. Energization of Outer Membrane Transport by the ExbB ExbD Molecular Motor. Vol. 205, Journal of Bacteriology. American Society for Microbiology; 2023.

75. Ames GFL. Bacterial Periplasmic Permeases as Model Systems for the Superfamily of Traffic ATPases, Including the Multidrug Resistance Protein and the Cystic Fibrosis Transmembrane Conductance Regulator. Int Rev Cytol. 1992 Jan 1;137(PA):1–35.

76. Qasem-Abdullah H, Perach M, Livnat-Levanon N, Lewinson O. ATP binding and hydrolysis disrupt the high-affinity interaction between the heme ABC transporter

HmuUV and its cognate substrate-binding protein. Journal of Biological Chemistry. 2017 Sep 1;292(35):14617–24.

77. Crofts AA, Poly FM, Ewing CP, Kuroiwa JM, Rimmer JE, Harro C, et al. Campylobacter jejuni transcriptional and genetic adaptation during human infection. Nat Microbiol. 2018 Apr 1;3(4):494–502.

78. Wilson T, Mouriño S, Wilks A. The heme-binding protein PhuS transcriptionally regulates the Pseudomonas aeruginosa tandem sRNA prrF1,F2 locus. Journal of Biological Chemistry. 2021 Jan 1;296.

79. Ullah I, Lang M. Key players in the regulation of iron homeostasis at the host-pathogen interface. Vol. 14, Frontiers in Immunology. Frontiers Media SA; 2023.

80. Sheldon JR, Himmel LE, Kunkle DE, Monteith AJ, Nichole Maloney K, Skaar EP. Lipocalin-2 is an essential component of the innate immune response to Acinetobacter baumannii infection. PLoS Pathog. 2022 Sep 1;18(9).

81. Kronstad JW, Caza M. Shared and distinct mechanisms of iron acquisition by bacterial and fungal pathogens of humans. Vol. 4, Frontiers in Cellular and Infection Microbiology. 2013.

82. Cassat JE, Skaar EP. Iron in infection and immunity. Vol. 13, Cell Host and Microbe. Cell Press; 2013. p. 509–19.

83. Taveirne ME, Theriot CM, Livny J, DiRita VJ. The Complete Campylobacter jejuni Transcriptome during Colonization of a Natural Host Determined by RNAseq. PLoS One. 2013 Aug 21;8(8).

84. Tikhomirova A, McNabb ER, Petterlin L, Bellamy GL, Lin KH, Santoso CA, et al. Campylobacter jejuni virulence factors: update on emerging issues and trends. Vol. 31, Journal of Biomedical Science. BioMed Central Ltd; 2024.

85. Bloomfeld SJ, Midwinter AC, Biggs PJ, French NP, Marshall JC, Hayman DTS, et al. Long-term colonization by campylobacter jejuni within a human host: Evolution, antimicrobial resistance, and adaptation. Journal of Infectious Diseases. 2018 Jan 1;217(1):103–11.

86. Li H, Limenitakis JP, Fuhrer T, Geuking MB, Lawson MA, Wyss M, et al. The outer mucus layer hosts a distinct intestinal microbial niche. Nat Commun. 2015 Sep 22;6.

87. Einhorn V, Haase H, Maares M. Interaction and competition for intestinal absorption by zinc, iron, copper, and manganese at the intestinal mucus layer. Vol. 84, Journal of Trace Elements in Medicine and Biology. Elsevier GmbH; 2024.

88. Murdoch CC, Skaar EP. Nutritional immunity: the battle for nutrient metals at the host–pathogen interface. Vol. 20, Nature Reviews Microbiology. Nature Research; 2022. p. 657–70.

89. Núñez G, Sakamoto K, Soares MP. Innate Nutritional Immunity. The Journal of Immunology. 2018 Jul 1;201(1):11–8.

90. Tourkochristou E, Triantos C, Mouzaki A. The Influence of Nutritional Factors on Immunological Outcomes. Vol. 12, Frontiers in Immunology. Frontiers Media S.A.; 2021.

Appendix

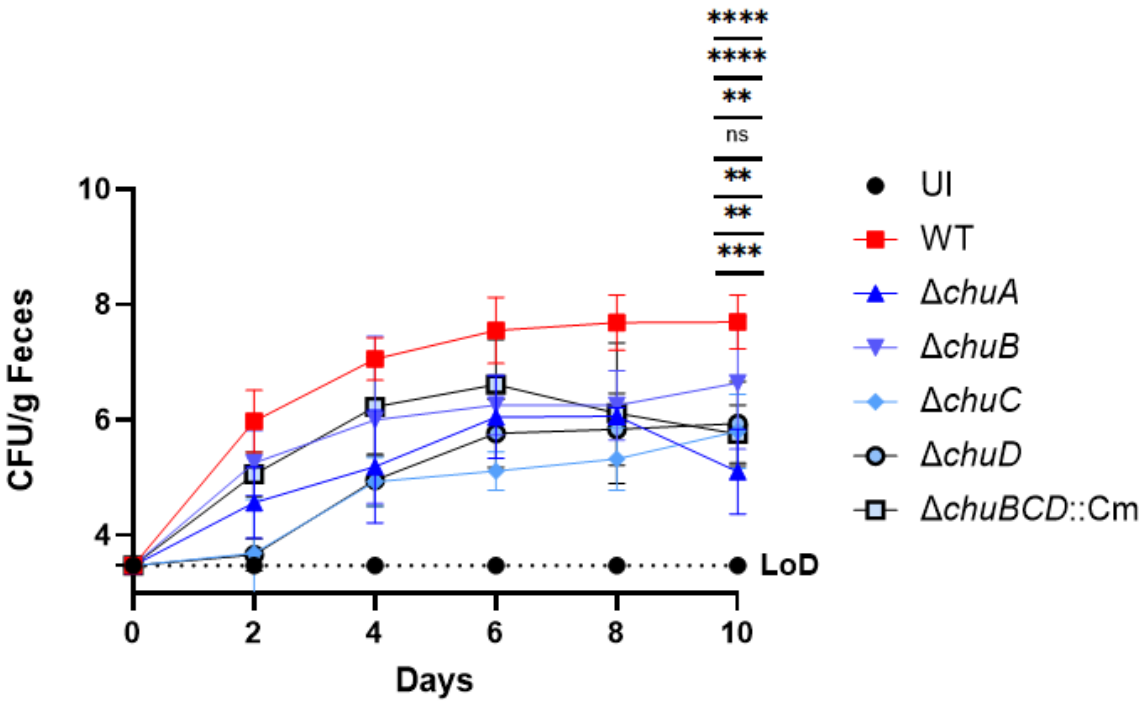

Figure 8: Colonization Trends Over 10-Day Infection. Colonization levels of wild-type and *chu* mutant strains in mouse feces over a 10-day infection period. CFUs were enumerated on *Campylobacter*-selective agar 72-hours after inoculation. Bacterial loads were quantified from fecal samples and reported as CFU/g. Strains tested include uninfected 1x PBS controls (UI, black circles), wild-type (WT, red squares), and *chu* deletion mutants: Δ*chuA* (blue upward triangles), Δ*chuB* (blue downward triangles), Δ*chuC* (blue diamonds), Δ*chuD* (gray circles), and Δ*chuBCD*::Cm (light blue open squares). The limit of detection (LoD) is indicated by the dotted line. Statistical analysis was performed using 2-way ANOVA with Tukey's multiple comparison test. Statistical significance compared to WT is shown in order of appearance in figure key: **** $p<0.0001$ (WT vs UI), **** $p<0.0001$ (WT vs Δ*chuA*), ** $p<0.01$ (WT vs Δ*chuB*), ns (WT vs Δ*chuC*), ** $p<0.01$ (WT vs Δ*chuD*), ** $p<0.01$ (WT vs Δ*chuBCD*::Cm). Data shown represents combined results from multiple independent experiments. Error bars represent standard error of the mean. Figure made using Prism10.

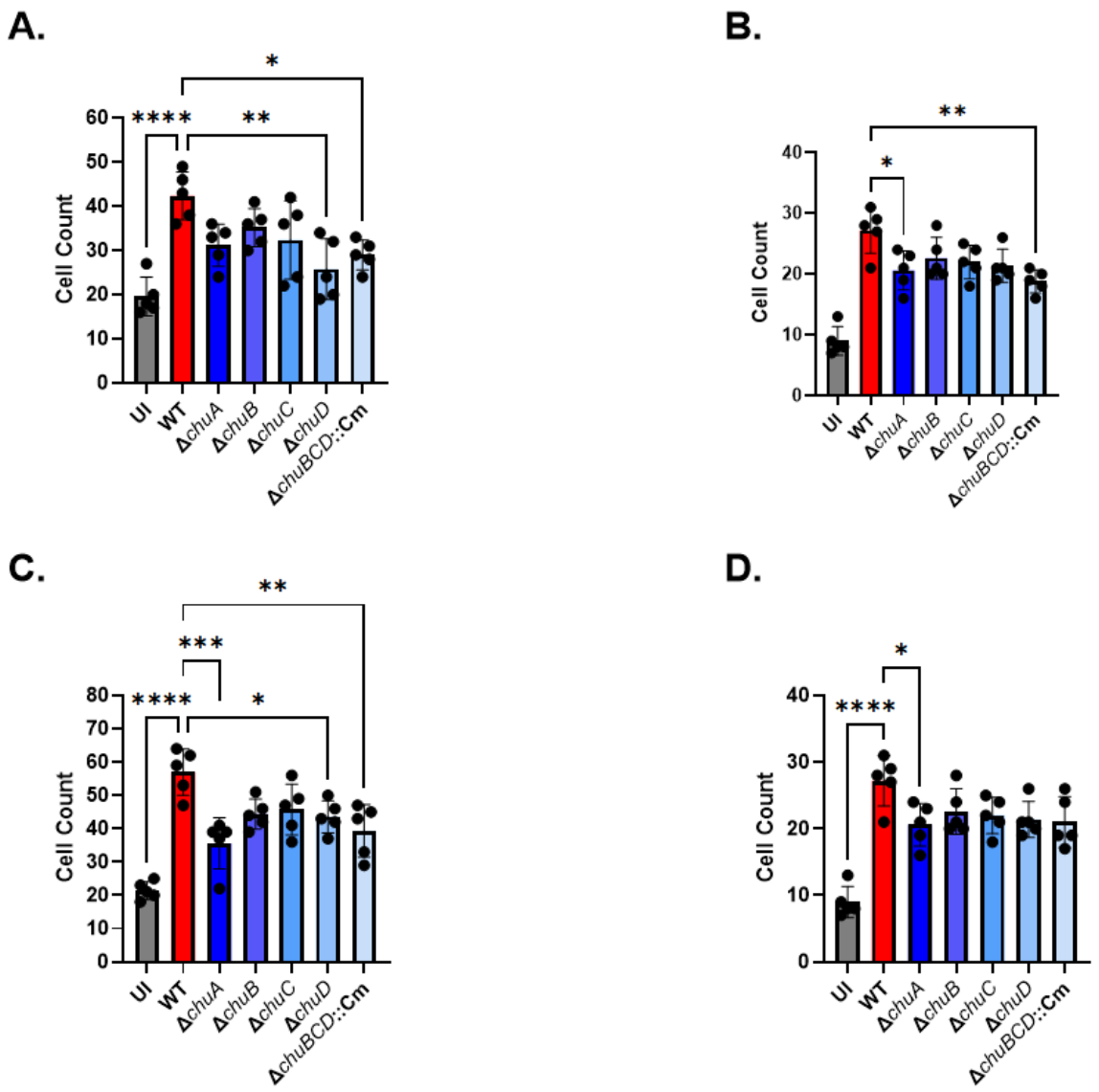

Figure 9: **Immune cell infiltration in IL-10 deficient mice infected with *C. jejuni* wild-type and *chu* mutant strains.** (A) Macrophage counts in cecal tissue sections showing significant increases in wild-type (WT) infection compared to uninfected (UI) controls (****p<0.0001) and reduced counts in *chu* mutants (*p<0.05, **p<0.01). (B) Macrophage counts in colonic tissue sections demonstrating elevated levels in WT infection (*p<0.05) and decreased counts in mutant strains (**p<0.01). (C) Neutrophil counts in cecal tissue showing marked increase in WT infection (****p<0.0001) compared to UI, with significant reductions in *chu* mutants (*p<0.05, **p<0.01, ***p<0.001). (D) Neutrophil counts in colonic tissue displaying increased infiltration in WT infection (***p<0.0001) and reduced counts in mutant strains (*p<0.05). All statistical analyses were performed using ordinary one-way ANOVA with multiple comparisons. Data points represent individual areas of tissue with means ± SEM (n=5 per group). Figure made using Prism10.

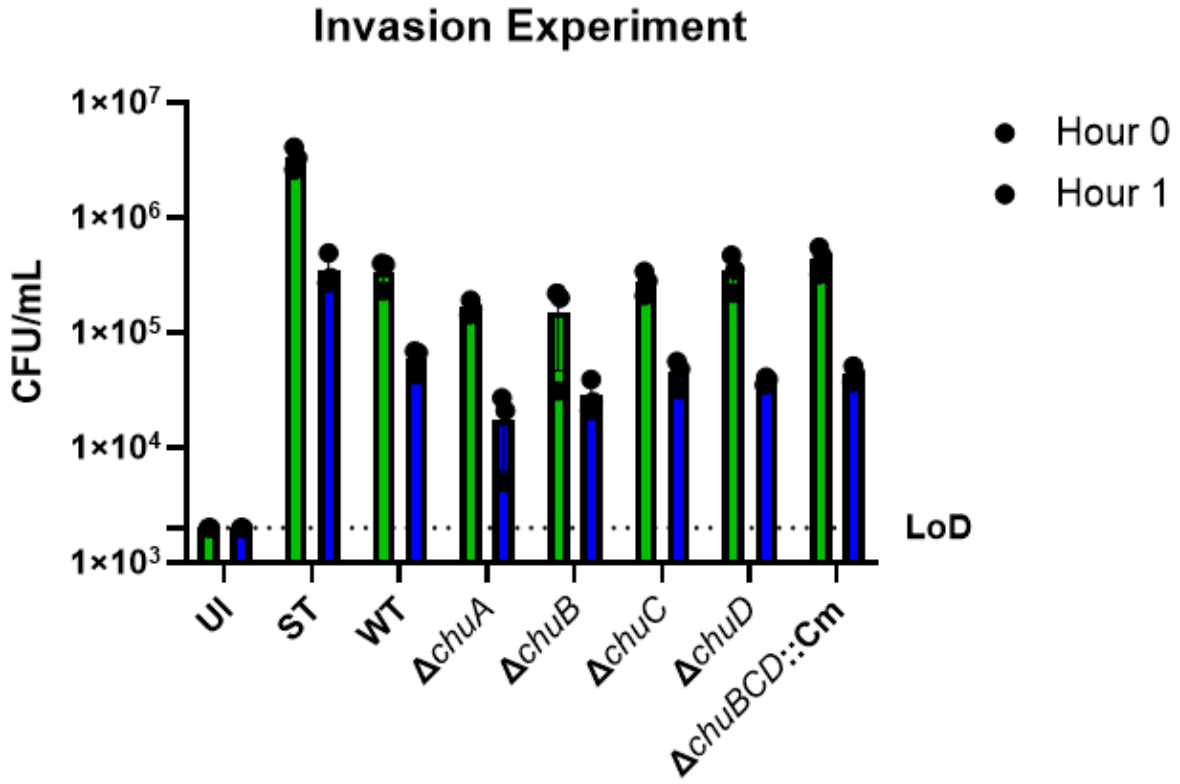

Figure 10: Invasion Assay Shows No Significant Difference Between Wild-type *C. jejuni* and Δ*chu* Knockout Mutant Strains. The invasion assay shows no significant difference between wild-type *C. jejuni* and Δ*chu* knockout mutant strains. The assay was performed using HCT116 cells in triplicate at two different time points. *Salmonella* enterica serovar Typhimurium (ST) was used as a control for positive cell invasion. Statistical analysis was conducted using a 2-way ANOVA followed by Tukey's multiple comparisons test. The results indicate that the deletion of the *chu* genes does not significantly affect the ability of *C. jejuni* to invade the intestinal epithelial cells. *$p < .1$*$p < .01$; ***$p < .001$; ****$p < .0001$. Figure made using Prism10.

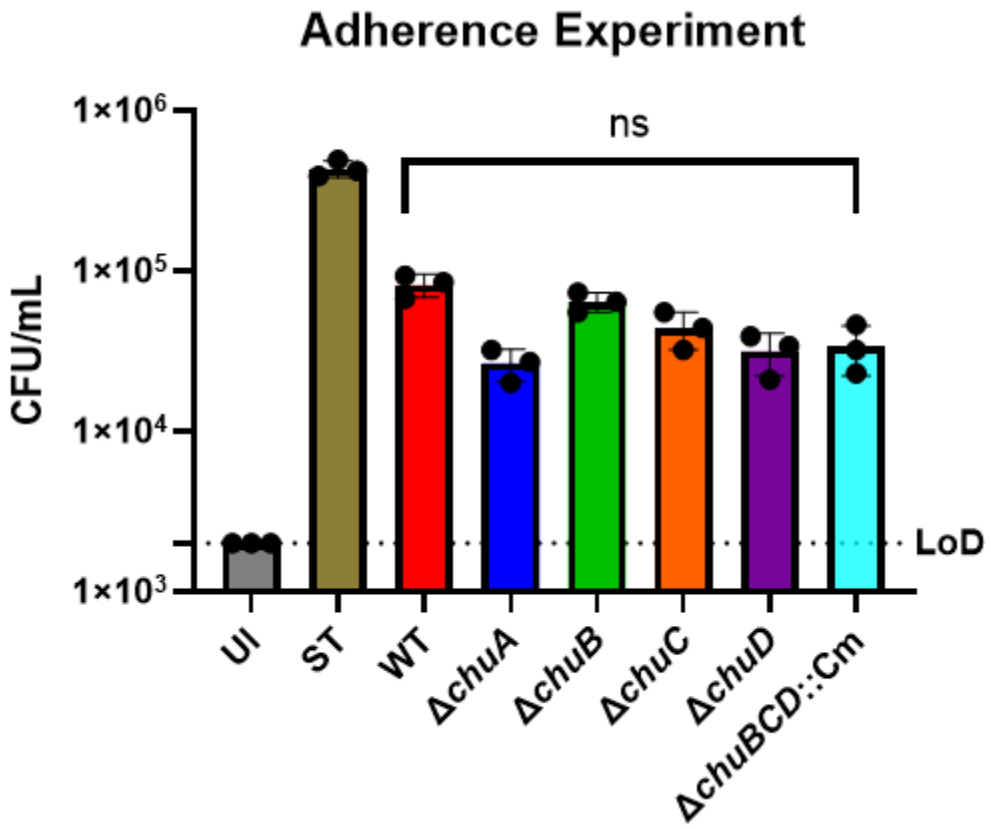

Figure 11: Assay Shows No Significant Difference Between Wild-type *C. jejuni* and Δ*chu* knockout mutant strains. The assay was performed using HCT116 cells in triplicate at two different time points to assess the adherence ability of the bacterial strains. *Salmonella enterica* serovar Typhimurium (ST) was used as a control for positive cell adhesion. Statistical analysis was conducted using a 2-way ANOVA followed by Tukey's multiple comparisons test. The results indicate that the deletion of the *chu* genes did not significantly affect the adherence properties of *C. jejuni* to the HCT116 cells. *p < .1*p < .01; ***p < .001; ****p < .0001. Figure made using Prism10.

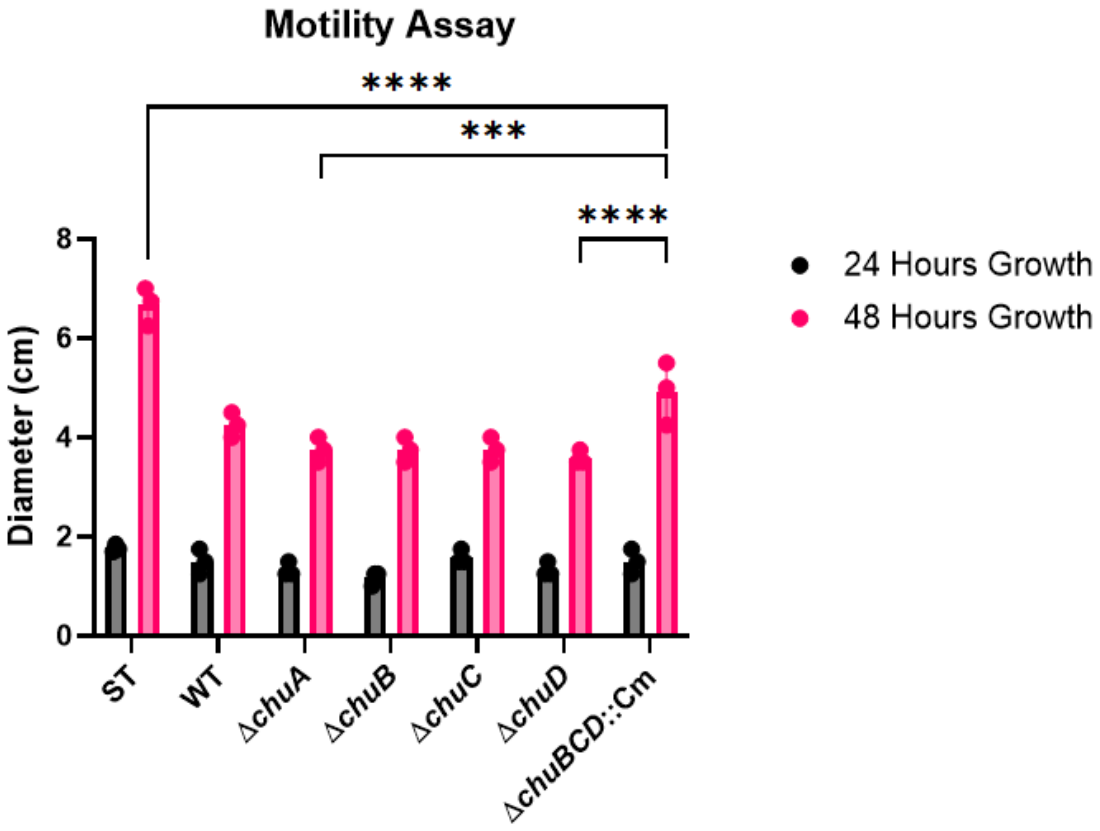

Figure 12: Motility Assay of Various Mutant Strains Over 24 and 48 Hours. The graph illustrates the motility of different cell strains, including *Salmonella enterica* serovar Typhimurium (ST), wild-type *Campylobacter jejuni* (WT), and mutant strains *(*Δ*chuA,* Δ*chuB,* Δ*chuC,* Δ*chuD,* and Δ*chuBCD*::Cm), measured as the diameter of growth (in cm) on motility plates. Black bars represent growth after 24 hours, while pink bars represent growth after 48 hours. Statistical analysis was performed using a 2-way ANOVA followed by Tukey's multiple comparisons test. All statistically significant values occurred during the 48-hour growth period. Statistical significance is indicated by asterisks (***$p < 0.001$, ****$p < 0.0001$), while the absence of statistical bars represents non-significant results. All samples were performed in triplicate, and error bars represent standard deviations from the mean. Figure made using Prism10.

Table 1: RT-qPCR Primers for *chu* and *rpoA* Gene Expression Analysis.

Table showing RT-qPCR primers designed for the quantification of *chu* and *rpoA* gene expression in *C. jejuni*. The sequences are listed for both forward and reverse primers, with *chu* primers targeting heme uptake genes and *rpoA* primers serving as a reference for normalization.

Primer Name	Sequence (5'-3')
chuA Forward	5'-CGGCATGAGAAATTCTCTATGTTTC-3'
chuA Reverse	5'-TTTTCATCTATAGCTCCCCACTTTT-3'
rpoA Forward	5'-GGTAGTAGAGGTGGCGTGATTA-3'
rpoA Reverse	5'-TTGTTTGCCACCATTCGATA-3'

Table 2: Representation showing the qPCR analysis of the *chuA* gene across each category of samples.

Data obtained is grouped into four main categories: Positive control, WT, UI, and Negative controls. Each sample had mean cycle threshold values ± SD for the amplification of *chuA* and *rpoA* genes. The relative expression of *chuA* calculated using the $2^{(-\Delta\Delta Ct)}$ method is presented in the rightmost column. Samples are sorted in the order from high to low relative *chuA* expression. From this, it can be concluded that the differential expression of *chuA* occurred across experimental conditions and tissues; generally, WT samples showed higher levels of expression.

Category	Sample	*chuA* Ct	*rpoA* Ct	Relative Expression
Positive	Positive control	22.36 ± 1.67	24.59 ± 1.64	4.70 ± 0.37
WT	WT colon	22.58 ± 1.62	24.23 ± 1.54	3.17 ± 0.44
WT	WT colon content	21.90 ± 1.20	22.29 ± 1.00	1.48 ± 0.76
UI	UI colon 2-Rep 6	35.56 ±	35.40 ±	0.90 ±
WT	WT cecum	29.77 ± 1.27	28.81 ± 0.93	0.73 ± 0.49
WT	WT cecal content	26.42 ± 1.39	25.65 ± 1.45	0.63 ± 0.26
UI	UI cecum 2-Rep 5	33.76 ±	32.86 ±	0.54 ±
UI	UI colon	33.91 ± 1.32	32.25 ± 2.37	0.39 ± 0.29
UI	UI cecum 2-Rep 4	33.19 ±	31.55 ±	0.32 ±
Negative	Negative control cecum	36.25 ± 2.09	33.66 ± 0.34	0.27 ± 0.32
UI	UI cecum 2	34.91 ±	32.81 ±	0.23 ±
UI	UI cecal contents	37.42 ± 2.28	32.77 ± 0.83	0.15 ± 0.28
UI	UI colon content	36.63 ± 1.80	32.78 ± 1.36	0.12 ± 0.11
Negative	Negative control colon	38.13 ± 1.55	33.40 ± 2.72	0.06 ± 0.06
UI	UI colon 2-Rep 5	38.49 ±	34.43 ±	0.06 ±
UI	UI cecum	38.39 ± 1.29	33.06 ± 1.54	0.03 ± 0.03
UI	UI colon 2-Rep 4	38.61 ±	32.09 ±	0.01 ±

Vita

Vincent Robert Randaisi, born in New Orleans in 1998, attended Shawnee State University from August 2016 to August 2021. He earned a Bachelor of Science degree in biological science with a minor in microbiology. During his time at Shawnee State, he spent two years researching tick populations in the Scioto area and screening them for *Borrelia burgdorferi*, the causative agent for Lyme disease.

In July 2022, Vincent began his graduate studies in the microbiology department at the University of Tennessee. While at UT, he worked in the Johnson lab and served as a graduate teaching assistant for courses in bioinformatics, general biology, and both general and advanced microbiology labs.